Final Report on ITER Task Agreement 81-08

Richard L. Moore

March 2008

INL
Idaho National Laboratory

The INL is a U.S. Department of Energy National Laboratory
operated by Battelle Energy Alliance

Final Report on ITER Task Agreement 81-08

Richard L. Moore

March 2008

Idaho National Laboratory
Idaho Falls, Idaho 83415

http://www.inl.gov

Final Report on ITER Task Agreement 81-08

INL/EXT-08-13894

March 2008

Approved by

(signature)

Richard L. Moore/Author

03/25/2008

Date

(signature)

Lee C. Cadwallader/Technical Checker

March 25, 2008

Date

(signature)

Brad J. Merrill/Peer Reviewer

3/25/08

Date

(signature)

Phil Sharpe/Approver/Manager

03/25/08

Date

ABSTRACT

As part of an ITER Implementing Task Agreement (ITA) between the ITER US Participant Team (PT) and the ITER International Team (IT), the INL Fusion Safety Program was tasked to provide the ITER IT with upgrades to the fusion version of the MELCOR 1.8.5 code including a beryllium dust oxidation model. The purpose of this model is to allow the ITER IT to investigate hydrogen production from beryllium dust layers on hot surfaces inside the ITER vacuum vessel (VV) during in-vessel loss-of-cooling accidents (LOCAs). Also included in the ITER ITA was a task to construct a RELAP5/ATHENA model of the ITER divertor cooling loop to model the draining of the loop during a large ex-vessel pipe break followed by an in-vessel divertor break and compare the results to a simular MELCOR model developed by the ITER IT. This report, which is the final report for this agreement, documents the completion of the work scope under this ITER TA, designated as TA 81-08.

ACRONYMS

AAS	Accident Analysis Specification
Be	Beryllium
CV	Control Volume
DV	Divertor
FPTS	Fusion Power Termination System
FW	First Wall
GSSR	Generic Site Safety Report
HS	Heat Structure
HX	Heat Exchanger
IB	Inboard
INL	Idaho National Laboratory
IT	International Team
ITA	Implementing Task Agreement
ITER	International Thermonuclear Experimental Reactor
LOCA	Loss of Coolant Accident
PHTS	Primary Heat Transport System
PT	Participant Team
RPrS	Report Preliminary on Safety
SADL	Safety Analysis Data List
SNAP	Symbolic Nuclear Analysis Package
TA	Task Agreement
TCWS	Tokamak Cooling Water System
VV	Vacuum Vessel

CONTENTS

Figures

1. INTRODUCTION

As part of an ITER Implementing Task Agreement (ITA) [1] between the ITER US Participant Team (PT) and the ITER International Team (IT), the INL Fusion Safety Program was tasked to provide the ITER IT with the following items : 1) upgraded fusion version of the MELCOR 1.8.5 and compare with early versions, 2) develop and include in MELCOR new ice layer/cryogenic model and upgrade the MELCOR model developed for the cryostat water/air/helium ingress , 3) provide required support and assistance in operation of the codes on request of ITER IT, 4) develop and include in the MELCOR code a hydrogen production model for high beryllium (Be) dust inventory (up to 100 kg) and upgrade the MELCOR model developed for the wet bypass event, 5) develop a RELAP5/ATHENA input deck for the ITER divertor cooling loop to model the large ex-vessel pipe break with air bypass, and compare results to a similar MELCOR model.

Task 1 of this ITA was completed and docummented in 2005 [2]. Task 2 listed above was completed and documented in 2006 [3]. The ice/cryogenic models discussed in Reference 3 are available in the present fusion version of MELCOR 1.8.5. The executables for this version of this code were sent to ITER IT after the completion of Task 2. Task 3 of the ITA was included to insure that the INL would provide the required support and assistance in the operation of the fusion version of the MELCOR 1.8.5 code. This phase of the TA 81-08 has been fulfilled.

The remaining two modeling tasks, Task 4 and 5 listed above are discussed in the following sections of this report. Section 2 presents the beryllium dust oxidation model developed under Task 4, and Section 3 presents the RELAP5/ATHENA model developed under Task 5. The final section of this report presents conclusions drawn from the work of the final tasks of this TA.

2. BERYLLIUM DUST OXIDATION MODEL

The purpose of this model is to allow the ITER IT to investigate hydrogen production from beryllium dust layers on hot surfaces inside the ITER vacuum vessel (VV) during in-vessel loss-of-coolant accidents (LOCAs). The accidents of concern are very small LOCAs that produce slow VV pressurization events that will not re-suspend this dust from these in-vessel surfaces.

2.1 Dust Layer Steam Oxidation

Reference 4 gives the following steady state, equimolar counter diffusion equation for Gas A (H_2O) into Gas B (H_2) when a chemical reaction occurs:

$$-D_{AB}\frac{d^2c_A}{d^2z} + R = 0 \tag{1}$$

where

D_{AB} is the binary diffusion coefficient of Gas A in Gas B (m^2/s)
c_A is the molar concentration of Gas A ($mole/m^3$)
z is the distance perpendicular to the dust film surface (m)
R is the bulk reaction rate ($mole$-H_2O/m^3-s)

For the case of a porous film, the binary diffusion coefficient in Equation 1 should be replaced by an effective diffusion coefficient that accounts for the porosity of the film and the tortuous diffusion path Gas A must make in order to diffuse through the film [5], defined as follows:

$$D_{eff} = \tau \varepsilon D_{AB} \tag{2}$$

where

τ is the tortuousity defined as the differential perpendicular distance of z to that of the actual path length $s = (dz/ds)^2$
ε is the porosity of the film

The bulk reaction rate of Equation 1 can be related to the INL beryllium/steam oxidation rate equations for full dense beryllium by adopting the specific surface area measured for beryllium dust by Reference [6], as follows:

$$R = s_D \rho_D R_{Be}^{INL} \kappa \tag{3}$$

where

s_D specific surface area for the dust particle (m^2/kg)
ρ_D dust density (kg/m^3)
R_{Be}^{INL} INL beryllium/steam oxidation rate equation for fully dense beryllium (kg-Be/m^2-s)
κ is a conversion factor from kg of Be to mole of H_2O for this reaction

The conversion factor κ equals 1000/9, and converts kg-Be to g-Be, g-Be to mole-Be, and accounts for the stoichiometry of the beryllium-steam reaction which is one mole of H_2O per mole of Be.

Reference 6 measured the specific surface area of five beryllium dust samples by the BET gas absorption technique. The results have been correlated (correlation coefficient of 98.9%) against the measured dust particle mass mean diameter, d_p (μm), giving the following linear fit:

$$s_D = 1693.7 - 33.6\, d_p \tag{4}$$

Figure 1 contains a comparison plot of the specific surface area data from Reference 6 and the predictions of Equation 4.

Reference 7 contains the INL beryllium-steam reaction equations for fully dense beryllium, which after conversion from STD liters of H_2/m^2-s to kg-Be/m^2-s are as follows:

$$
\begin{aligned}
R_{Be}^{INL} &= 1.205 \times 10^{-1} e^{-13465/T} & T &< 793K \\
R_{Be}^{INL} &= 2.571 \times 10^{7} e^{-28789/T} & 793K &< T < 1133K \\
R_{Be}^{INL} &= 3.536 \times 10^{1} e^{-13387/T} & T &> 1133K
\end{aligned}
\tag{5}
$$

The INL beryllium-steam reaction equations were developed at a steam pressure of 0.86 atm. In SADL [8], it is assumed that the beryllium-steam reaction will vary as steam pressure raised to the 0.9 power ($p^{0.9}$). We can approximate this assumption by allowing for a first-order chemical reaction defined as:

$$R = k\, c_a \tag{6}$$

where reaction rate coefficient k is related to Equation 3 as follows:

$$k = \frac{s_D\, \rho_D\, R_{Be}^{INL} \kappa}{c_{H2O}} \tag{7}$$

where c_{H2O} is the molar concentration of the steam at the INL test conditions (27.7 mole/m^3).

With these definitions, Equation 1 becomes

$$-D_{eff}\frac{d^2 c_A}{d^2 z} + k\, c_A = 0 \tag{8}$$

Reference 9 solves this equation for boundary conditions of a defined concentration at z equals zero of c_A^o and a non-flow boundary at z equal the layer thickness, δ (m), to obtain the steam concentration profile in the film as:

$$c_A = c_A^o \left[\cosh\left(\sqrt{k/D_{eff}}\ z\right) - \tanh\left(\sqrt{k/D_{eff}}\ \delta\right)\sinh\left(\sqrt{k/D_{eff}}\ z\right)\right] \tag{9}$$

We can now derive a steam reaction rate based on the geometric surface area of the film R_s (kg-Be/m²-s) by substituting Equation 9 into Equation 6, and integrating over the thickness of the film. The resulting equation is:

$$R_s = \frac{k\,c_A^o}{\kappa\sqrt{k/D_{eff}}}\left\{\sinh\left(\sqrt{k/D_{eff}}\,\delta\right) + \tanh\left(\sqrt{k/D_{eff}}\,\delta\right)\left[1\text{-}\cosh\left(\sqrt{k/D_{eff}}\,\delta\right)\right]\right\}$$

$$= \frac{k\,c_A^o}{\kappa\sqrt{k/D_{eff}}}\tanh\left(\sqrt{k/D_{eff}}\,\delta\right) \tag{10}$$

What remains to be defined are the binary diffusion coefficient, and the film properties of porosity, particle diameter and film thickness. Reference 10 gives the following formula for the diffusion of H_2O into H_2:

$$D_{AB} = D_{AB}^o\left(\frac{p_o}{p}\right)\left(\frac{T}{T_o}\right)^{3/2}\frac{\Omega_{T_o}}{\Omega_T} \tag{11}$$

where

        D_{AB}^o is a measured binary diffusion coefficient for steam in hydrogen at pressure p_o = 1 atm and temperature T_o = 293 K equal to 8.5×10^{-5} m²/s for steam in hydrogen

        Ω_T is the Lennard-Jones collision integral

Fortran functions subroutines that contain this oxidation model appear in Appendix A. These subroutines were developed for application with the MELCOR code.

Based on a recent communication, the dust layer (film) density is to be assumed as 1 g/cm³ and the film thickness as 2 mm [11]. At this density, the layer porosity is 0.45. If the dust particle diameter is set at the mass mean diameter for dust callout in SADL [8] of 2 μm, then all of the quantities necessary to allow a comparison between Equation 10 and the INL beryllium-steam oxidation rate equations for fully dense beryllium have been defined. This comparison appears in Figure 2. Also presented in this figure are the measured INL oxidation rates for beryllium dust and 88% dense beryllium from References 6, 12 and 13. The dust data presented assumes a specimen geometric surface area equal to that of the crucible that the tests were conducted in. As can be seen, the reaction rate from Equation 10 for 2 μm particles is greater than either fully dense or 88% dense beryllium over the temperature range investigated. There is also some agreement between the dust reaction rates measured at 400°C and the prediction of Equation 10 for a dust density and particle size more typical of that of the INL dust (0.7 g/cm³ and 20 μm).

Figure 3 illustrates the diffusion depth of water in a 2 mm beryllium layer as a function of layer temperature for this oxidation model. What is plotted in this figure is the predictions of Equation 9 divided by the left-side boundary condition c_A^o. Below 600°C the limiting rate process appears to be surface oxidation of the dust particles. It is not until 900°C that steam diffusion begins to significantly limit the reaction rate in the back half of the layer.

2.2 Dust Layer Effective Thermal Conductivity

The effective thermal conductivity of the beryllium dust layer is based on a correlation developed for pebble bed fission reactors [14]. As described in Reference [14] the overall effective conductivity is calculated from three different individual effective conductivities. The individual effective conductivities are summed to obtain the overall effective conductivity of a given region. These three individual effective conductivities are defined as (1) void radiation plus solid conduction, (2) gas conduction plus solid conduction, and (3) contact conduction plus solid conduction.

Equation (12) describes the effective conductivity due to void radiation plus solid conduction and is based on the cell model defined by Zehner and Schlünder [15] and modified by G. Breitbach and Barthels [16].

$$\lambda_{er} = \left[\left(1 - \left(1-\varepsilon_p\right)^{\frac{1}{2}} \right) \cdot \varepsilon_p + \left(\frac{\left(1-\varepsilon_p\right)^{\frac{1}{2}}}{\frac{2}{\varepsilon_r}-1} \right) \cdot \frac{B+1}{B} \cdot \frac{1}{1+\frac{1}{\left(\frac{2}{\varepsilon_r}-1\right)\cdot\Lambda}} \right] \cdot 4\sigma T^3 d \qquad (12)$$

where

$$B = 1.25\left(\frac{1-\varepsilon_p}{\varepsilon_p} \right)^{\frac{10}{9}} \qquad (13)$$

$$\Lambda = \frac{\lambda_s}{4\sigma T^3 d} \qquad (14)$$

The variables in Eq.'s (12), (13) and (14) are σ the Stefan-Bolzmann constant, λ_s the thermal conductivity of beryllium, ε_p the porosity of the pebble bed (0.55), ε_r the emissivity of the beryllium dust (0.3), d the mean diameter of the dust particles (2.1 μm), and T is the average temperature of the dust particles in the control volume.

The second term describes the effective conductivity due to gas conduction plus solid conduction. This equation was formulated by Zehner and Schlünder and tested by V. Prasad et, al [17].

$$\lambda_{eg} = \left[1 - \sqrt{1-\varepsilon_p} + \frac{2 \cdot \sqrt{1-\varepsilon_p}}{1-\lambda \cdot B} \cdot \left(\left(\frac{(1-\lambda) \cdot B}{(1-\lambda \cdot B)^2} \right) \cdot \ln\left(\frac{1}{\lambda \cdot B} \right) - \left(\frac{B+1}{2} \right) - \left(\frac{B-1}{1-\lambda \cdot B} \right) \right) \right] \cdot \lambda_g \quad (15)$$

where

$$\lambda = \frac{\lambda_g}{\lambda_s} \quad (16)$$

In equations (15) and (16) λ_g is the thermal conductivity of gas in the space between the pebbles in the pebble bed.

The third term describes the effective conductivity due to contact conduction between dust particles plus solid conduction within the pebbles. The effective conductivity component is the result of compressive loads on the spheres due to the weight of the particles in the dust layer.

$$\lambda_{ec} = \left[\frac{3 \cdot (1-\mu_p^2)}{4 \cdot E_s} \cdot f \cdot \frac{d}{2} \right]^{\frac{1}{2}} \cdot \frac{1}{0.531 \cdot S_s} \cdot \left(\frac{N_A}{N_L} \right) \cdot \lambda_s \quad (17)$$

where

$$f = p \frac{S_F}{N_A} \quad (18)$$

For a bed assumed to have a simple cubic arrangement of the spheres, S_S, S_F, N_A and N_L are given as $S_S = 1$, $S_F = 1$, $N_A = 1/(4R^2)$, $N_L = 1/(2R)$ where R is the radius of a particle. In Eq. (17) $\mu_p = 0.032$ and $E_S = 287 \times 10^9$ (N/m^2). These two values are Poisson's ratio and Young modulus, respectively. The variable p is the external pressure and is estimated by the weight of the pebbles in the pebble bed.

The effective thermal conductivity of the dust layer is the sum of the three terms given above:
$$k_{eff} = \lambda_{er} + \lambda_{eg} + \lambda_{ec} \quad (19)$$

The above equations were programmed into Mathcad [18] using temperature dependent steam [19] and beryllium [8] thermal conductivities to generate the effective thermal conductivity used in this oxidation model. The generated effective thermal conductivity is shown in Figure 4.

2.3 Initial MELCOR Dust Layer Test Case

As an initial test case simulating the introduction of steam into the ITER vacuum vessel at the end of a plasma pulse was examined to ascertain the response of this beryllium dust oxidation model. A MELCOR input deck was developed for this test case by extracting component from a

MELCOR input deck used for the ITER-FEAT Generic Site Safety Report [20]. These components include the inboard (IB) first wall (FW), the cooling volume for the FW, and the VV volume. FW heating surface and nuclear heating was included in the model. The thermodynamic properties of VV volume for this test case where defined through user input to give a vacuum during the power pulse, followed by a steam environment at one atmosphere within one second of the pulse termination. Because the beryllium dust oxidation model has not been incorporated into the MELCOR code, the response of this model was simulated by two MELCOR user functions that returned oxidation rate and surface heating. To illustrate the impact of this model, a second inboard FW structure was added to this model that contained a 2 mm thick dust layer on the VV side of this wall, to the surface of which the additional chemical heating was added. A copy of this MELCOR input deck can be found in Appendix B.

Figure 5 illustrates the impact that a 2 mm beryllium dust layer would have on the IB FW. The dust layer surface temperature is 700 K hotter than an IB FW surface without a dust layer due to the low effective thermal conductivity of this dust layer. The consequence of this higher temperature is an immediate ignition of the dust layer once steam fills the VV, as can be seen in Figure 6. Because this condition is a function of the heat transfer conditions available to this layer (e.g., surface convection, surface thermal radiation, and conduction to the beryllium substrate of the FW), parameter studies were undertaken to determine how high the dust layer conductivity would have to be to avoid ignition for these pseudo-accident conditions of this test case. As can be seen, if the effective conductivity of the dust layer were to be increased by a factor about 2.5, then the energy balance is such that ignition is avoided.

It should be noted that this test case does not represent a real accident condition for ITER-FEAT, but has been used in this summary report to demonstrate the progress that has been made regarding this model's development. Should the ITER IT approve of this beryllium dust layer oxidation model, then it will be incorporated into the MELCOR code so that more realistic accident scenarios can be examined.

2.4   Application of Dust Layer to ITER Wet Bypass Scenario

The postulated initiating event for this accident is an ex-vessel divertor primary heat transport system (PHTS) pipe break. A description of this accident can be found in the GSSR-Volume 7 [20]. It is postulated that during a plasma burn, a double-ended pipe rupture of the largest pipe (total flow area of ~0.4 m^2) is assumed to occur in the ex-vessel section of a divertor primary heat transfer system coolant loop (DV ex-vessel coolant pipe break). Coolant is discharged at a high rate into the heat transfer system vault. The fusion power termination system will actuate on a high pressure signal from a pressure sensor in the vault or low pressure signal from a pressure sensor in the primary cooling system, terminating the plasma burn by five seconds into this event. Even though the plasma burn is terminated, there is a possibility that the divertor cooling channels will undergo damage by melting due to the high heat flux before plasma termination.

One task of the ITA is to apply this dust layer model to the GSSR ITER Wet Bypass accident. The MELCOR input deck modified for this application was obtained from the ITER IO and was that used for analyzing this accident in the GSSR [20]. The modifications made to this deck, called "feat2001.divsim.inp", appear in Appendix C. Several assumptions had to be made in order to apply this dust layer model to this accident. The first assumption was whether or not the dust layer (100 kg is to be considered according to the ITA) resides over the entire surface of ITER FW beryllium tiles or if the dust layer lies in the grooves between FW beryllium titles. If

100 kg of dust is distributed over the entire FW surface area (680 m^2) then the depth of this dust layer (density = 1000 kg/m^3) would be ~0.15 mm. Given the results of the previous section, a dust layer that is 0.15 mm thick will probably not undergo a thermal runaway during the transient conditions predicted for a wet bypass accident. The surface area of the groves between tiles is estimated to be ~36 m^2. This area estimate is based on a FW tile dimension of 53.4 mm x 53.4 mm x 10 mm, with a gap between tiles of 1.5 mm [21]. Based on these dimensions, there are ~225,600 FW tiles, which results in a gap area of 36.6 m^2. A dust layer of this surface area would have a thickness of ~2.8 mm. Based on the results of the previous section, a dust layer of this thickness could undergo a thermal runaway during a wet bypass accident provided that:

1) the dust layer experiences the same surface heating as the rest of the FW, an assumption that conservatively ignores the shadowing effect of the thicker beryllium tile (10 mm thick), and
2) the heat transfer between the Be dust and Be tiles or copper substrate is sufficiently low.

The second assumption involves interface heat transfer between the dust and the tiles or copper substrate. Typically, heat transfer at such interfaces is modeled with a gap conductance heat transfer coefficient. It is assumed here that this approach is applicable to a dust-tile or dust-substrate interface. However, a correlation for dust gap conductance coefficients was not found in literature.

Reference 22 does present an overview of the effects of gas pressure and mechanical load on the thermal gap conductance. This reference compares the predictions of eight gap conductance correlations against data from stainless steel and nickel alloy gap conductance tests. As demonstrated in this article (note Figure 7 which is a reproduction of Figure 3 from Reference 22), the thermal conductance of a gap decreases with gap gas pressure and with the mechanical load used to press the two metal surfaces together. The reported variation with gap gas pressure shows a decrease in gap conductance from 4 kW/m^2-K for nitrogen in the gap at a pressure of 100 kPa to 0.6 kW/m^2-K for a gas pressure of 1.3 kPa for the lowest mechanical load studied (~400 kPa). Since the gap conductance is thought to be the sum of two contributions, that from metal contact plus that from the interstitial gas conduction in the gap [23], then by lowering the gas pressure as shown in Reference 22 the gas contribution to the gap conductance would be less. This would suggest that the gas contribution was on the order of 3.4 kW/m^2-K for this tests.

Reference 23 suggests that the gas contribution (h_g, W/m^2-K) can be estimated based on the gas thermal conductivity (k_g, W/m-K) by the following equation:

$$h_g \approx \frac{k_g}{2.7\sigma} \tag{20}$$

where σ (m) represents the effective root mean square surface roughness at the gap defined as:

$$\sigma = \sqrt{\sigma_1^2 + \sigma_2^2} \tag{21}$$

where the subscripts (1, 2) refer to the two materials forming the gap. Applying Equation 20 to the test conditions reported in Reference 20, the gas contribution to the gap conductance would be ~4.0 kW/m^2-K, which is close to that suggested by the data for Experiment 1 of Reference 22.

However, since the thermal conductivity of a mono-atomic gas is in theory independent of pressure for collisional gases [24], the dramatic fall off in reported gap conductance with pressure below 27 kPa cannot be simulated with Equation 20 by merely using measure nitrogen gas thermal conductivities. However, if a formula for effective gas conductivity in powder beds, cited in Reference 25, is used in Equation 20, then the correct trend can be obtained. This formula is as follows:

$$k_g^{eff} = \frac{k_g}{\dfrac{B}{p_g \sigma} + 1} \tag{22}$$

where p_g is the gas pressure (Pa). The coefficient B of Equation 22 is defined as

$$B = \frac{4\gamma}{\gamma + 1} \frac{2 - A}{A} \frac{\Lambda_o p_o}{Pr} \tag{23}$$

where

γ	-	gas specific heat ratio
A	-	gas accommodation coefficient (taken as 1)
Λ_o	-	molecular mean free path (m) of gas at pressure p_o
p_o	-	reference pressure (set at 100 kPa)
Pr	-	gas Prandlt number

When the thermal conductivity of Equation 22 is used in Equation 20, then the predicted gap gas conductance for the test conditions of Experiment 1 of Reference 20 is 3.6 kW/m^2-K at 100 kPa (760 torr), 2.2 kW/m^2-K at 13.3 kPa (100 torr), and 0.4 kW/m^2-K at 1.3 kPa (10 torr). These coefficients are in agreement with those cited in Figure 3 of Reference 20. While the correct gap conductance could lie within this range of values, this study will investigate the response of the dust layer to a range of gap conductances to understand the predicted gap conductance required to avoid a thermal runaway condition.

Lateral conduction from the dust layer to the FW tiles is calculated using the following formula for the overall heat transfer heat coefficient (h_o, W/m^2-K) between the dust and the tile:

$$h_o = \frac{1}{\dfrac{\delta_T}{k_T} + \dfrac{1}{h_{gap}} + \dfrac{\delta_D}{k_D}} \tag{24}$$

where

δ	–	lateral distance heat is being conducted (m)
k	-	thermal conductivity (W/m-K)
h_{gap}	-	gap conductance coefficient (W/m^2-K)
D,T	-	subscripts denoting dust (D) and tile (T).

This dust lateral heat conduction is simulated through user functions in the MELCOR input file. A schematic of the 2D dust heat conduction model simulated through these user functions appears in Figure 8. The radial conductors are those of the normal MELCOR 1D heat conduction solution for MELCOR heat structures. As illustrated, there are three 1D heat structures in this

model, one simulating radial heat conduction through the Be tile and adjoining Cu substrate and two for the Be dust and adjacent Cu substrate. The changes made to the GSSR MELCOR input model for the Wet Bypass accident to incorporate this dust layer conduction model appear in Appendix B.

Figure 9 contains the predicted dust layer surface temperature for gap conductance heat transfer coefficients of 500 W/m^2-K, 250 W/m^2-K, and 100 W/m^2-K. As can be seen, thermal runaway occurs for a gap coefficient of 100 W/m^2-K. There are two temperature histories for a gap coefficient of 100 W/m^2-K. The first history is for a case where beryllium evaporation is allowed to occur. This evaporation carries heat away from the surface, and thereby limits the surface temperature. For this case, the dust oxidation terminates as result of a complete oxidation of the dust layer. The second history is for a case that assumes that the dust oxidation is occurring primarily at the surface of the dust layer at high temperatures (a good assumption in light of the results presented in Figure 3). As a result, this surface oxidation will produce a growing beryllium oxide layer through which steam will have to diffuse before it could react with the beryllium beneath the developing oxide film. For this case 80% of the dust layer oxidizes before the produced oxidation energy falls below the energy lost by heat conduction to the Be tiles or Cu substrate.

The question becomes: what would be a good choice for this gap conductance? If the gap conductance is assumed to be only by the way of the gas in the gap (e.g., Equation 20), then the result shown in Figure 10 is obtained. As can be seen in this Figure, initial the dust layer temperature is very high (~1400 K) because the only mode of heat transfer at the gap is radiation heat transfer. However, soon after the steam enters the VV by way of the in-vessel divertor break, the enhanced gap conductance provides a cooling rate by way of the FW tiles that is greater than the heat production due to chemical oxidation of the dust layer, resulting in a rapid drop in dust layer temperature as opposed to a thermal runaway in the dust layer. The predicted gap conductance heat transfer coefficient for the dust layer during this accident given in Figure 11. While it would appear from these results that the auto-ignition of the dust layer is unlikely, further research into dust oxidation and heat transfer is required to confirm these results.

3. MELCOR AND RELAP5/ATHENA MODELS

Also included in this ITER ITA is a task to construct a RELAP5/ATHENA model of the ITER divertor cooling loop to model the draining of the loop during a large ex-vessel pipe break followed by an in-vessel divertor break. Draining the loop this way results in an air bypass between the VV and the Tokamak Cooling Water System (TCWS) vault, through which tritium and activated dust from the VV can be transported into the TCWS vault. A MELCOR model for this accident has already been developed; however, the ITER IT wanted to compare the results obtained from a RELAP5/ATHENA model with the MELCOR model results because a previous ATHENA model of the first wall blanket cooling loop (FW/BLK) predicted much faster draining of the FW/BLK loop than a similar MELCOR model. The comparision of the results obtained from the two models should help resolve the discrepancy between ATHENA and MELCOR models of similar accidents.

3.1 MELCOR Model

The MELCOR model (input deck feat2004.divsimpf.inp) of the divertor ex-vessel pipe break whose results are to be compared to results from a comparable RELAP5/ATHENA model that was obtained from the ITER IO. The accident being modeled is a postulated double ended pipe break in the divertor cooling loop downstream of the divertor loop pump (see Figure 12). Since the location of the pipe where the break occurs is in the TCWS vault, the coolant from the ex-vessel break will discharged into the TCWS vault causing a presssure increase in this vault. The plasma is postulated to continue to burn until terminated by the fusion power termination system (FPTS), ~ 3 seconds after the initiation of the ex-vessel break. The termination of the plasma burn causes a plasma disruption followed by a break in the divertor (DV) cooling pipes, allowing coolant to discharge into the VV. A more detailed description of this accident can be found in the accident analysis specification (AAS) [26] document.

Figures 12, 13, and 14 contain schematics of the MELCOR models for the divertor cooling loop, the suppression system and the vault system, respectively. The divertor cooling loop model shown in Figure 12 contains the divertor loop pump, the loop heat exchanger, the hot collector, the cold distributor, the divertor cassettes, the pressurizer, and the piping connecting the main components. Also shown in the figure are the locations of the assumed ex-vessel break and the resulting in-vessel break.

The ex-vessel double ended guillotine break is simulated in the model by using flow paths 38 and 39 which contain valves that are programed to immediately open at the time the accident is initiated. Flow path 38 connects the upstream side of the break (CV435) to the TCWS vault while flow path 39 connects the downsteam side of the break (CV425) to the TCWS vault. An isolation valve is used in flow path 415 to isolate the upstream side of the break from the downstream side of the break. The isolation valve is programed to immediately close at the time the accident is initiated.

The in-vessel break is simulated using two flow paths, 36 and 37. These two break flow paths (shown in Figure 12) connect divertor components CV413 and CV417 to the vacuum vessel

CV100 by way of CV450. Valves in the two flow paths are programed to start opening five seconds after the initiation of the accident and to become fully open at seven seconds.

The suppression system (see Figure 13) and the vault system (see Figure 14) are an integral part of the divertor loop model due to the fact that the ex-vessel break mass flow discharges into the TWCS vault and the in-vessel break mass flow discharges into the plasma chamber. The VV (plasma chamber) is connected to the suppression system by a number of flow paths. The suppression system consists of two main components, the suppression tank (CV102) and the drain tank (CV122) and the piping needed to connect the suppression tank and the drain tank to the plasma chamber. The vault system (see Figure 14) consists of the TWCS vault, the pipe chase, the gallery, and the NBI cell.

The above figures were generated by importing the MELCOR input deck for the large ex-vessel break with air bypass (feat2004.divsimpf.inp) into the Symbolic Nuclear Analysis Package (SNAP) [27]. This package is under development by Applied Programming Technology, Inc. for the US Nuclear Regulatory Commission. The package is intended to provide a consistent and easy to use interface to design and build input models and analyze output from codes such as MELCOR and RELAP5/ ATHENA.

3.2   RELAP5/ATHENA Model

As requested in the ITA, a RELAP5/ATHENA model was developed which models the large ex-vessel pipe break with air bypass similar to the MELCOR model presented above. The model was developed using the RELAP5 modeling capabilities that are an integral part of the SNAP program. Geometric data in the form of volumes, cross-sectional areas, flow path lengths, component elevations, heat structure thicknesses, etc., used to construct the model were obtained from the MELCOR computer model described in Section 3.1 and entered into the SNAP program to generate a corresponding RELAP5/ATHENA model. Also obtained from the MELCOR model were the time and spatial distribution of heating loads that were applied to the RELAP5 heat structures.

Shown in Figure 15 is a schematic of the RELAP5/ATHENA model that was generated using the SNAP program. In order to get a better view of the model presented in Figure 15; the figure was split in the middle with the right hand side of Figure 15 shown in Figure 16 and the left hand side of Figure 15 shown in Figure 17. The RELAP5/ATHENA suppression and vault system models are shown in Figures 18 and 19, respectively. These two models correspond to the MELCOR suppression and the vault system models shown in Figures 13 and 14, respectively.

Not shown or discussed in the MELCOR section is the FW primary heat transport system (PHTS) which interacts only with the DV coolant loop through radiation heat transfer and any water/steam injected into the VV by convection heat transfer since the FW PHTS remains intact during this accident. Therefore, the FW PHTS was included in the RELAP5/ATHENA model as a FW heat structure with a time dependent water temperature boundary condition obtained from the MELCOR model results.

Comparing Figures 13 and 14 to Figures 18 and 19, respectively, we see that not all the leak paths in the MELCOR suppression and vent system models are modeled in detail in the RELAP5/ATHENA model. The leak paths not modeled in detail in the RELAP5/ATHENA model are modeled as boundary conditions using time dependent junctions connected to time dependent volumes using leak flow rates predicted by MELCOR.

3.3   Comparison of MELCOR and RELAP5/ATHENA Results

The initiating event for this transient is a double ended ex-vessel pipe break into the TCWS vault followed by an in-vessel break into the VV. The ex-vessel break is assumed to occur at 1000 seconds into the transient. The first 1000 seconds of transient time allows the DV coolant loop to obtain a steady state condition before the initiating of the ex-vessel break. Shown in Figure 20 is a comparision of the predicted MELCOR and RELAP5/ATHENA total mass flow rate time history of the DV loop. The predicted MELCOR and RELAP5/ATHENA steady state loop mass flow rates (time < 1000 second) were 1019 kg/sec and 1037 kg/sec, respectively, a 1.7% difference. This time history was taken just upstream of the loop Hx.

At time equal to 1000 seconds the ex-vessel break is programmed to occur. The total break mass flow rates for both the MELCOR (flow paths 38 and 39) and the RELAP5/ATHENA (valves 38 and 39) models are shown in Figure 21. Overall the predicted mass flow rate from MELCOR is slightly higher as evidenced in Figure 22 which shows the total integrated mass flow (water, steam, and air) through the ex-vessel break for both models. The predicted total mass flow to the TCWS vault based on the MELCOR model was 55000 kg compared to 51500 kg predicted by the RELAP5/ATHENA model. The peak integrated mass flows occurred at 1200 and 1850 second respectively. The reduction in peak mass to the TCWS vault as seen in the figure is due to air flowing from the vault to the VV once the DV loop pressure drops below that of the vault as a result of a flow path that develops through the ex-vessel in-vessel breaks by way of the partially voided DV coolant loop. The difference in the timing of the air entering the VV is probably due to the differences in the inter-phase drag correlations used in these two codes.

The mass flow rates corresponding to the in-vessel break which is programmed to occur five seconds after the ex-vessel break are presented in Figure 23. Initially the mass flow rate predicted by MELCOR is slightly higher than that predicted by RELAP5/ATHENA as seen in Figure 24 which shows the integrated mass flow through the in-vessel break for both models. The MELCOR integrated mass flow rapidly approaches 61500 kg at 1335 seconds, then gradually increases to 64000 kg at the end of 5000 seconds. The RELAP5/ATHENA results show the integrated mass flow reaching 65500 kg at 2150 seconds, then gradually increasing to 66200 kg at the end of 5000 seconds. This difference in the timing of the initial peak total mass flow between the two models is again attributed to the difference in the inter-phase drag correlation used in these codes.

The pressures in the TCWS vault and VV (plasma chamber) are shown in Figure 25 for both the MELCOR and RELAP5/ATHENA models. The pressure in the VV rises rapidly to the pressure suppression system opening set point of 150 kPa in both cases. It takes ~20 seconds for the MELCOR model to reach the set point following the in-vessel break where as the RELAP/ATHENA model takes ~ 30 seconds. After the pressure suppression system opens the predicted pressure corresponding to the RELAP5/ATHENA model drops lower and takes longer to recover (pressure equilibrium between TCWS vault and the VV) than for MELCOR. The pressure recovery in the VV is due to the inflow of air from the TCWS vault into the VV. As indicated in Figure 25 the flow of air from the TCWS vault to the VV begins at ~1200 seconds for MELCOR and ~1700 seconds for RELAP5/ATHENA. The peak pressure in the TCWS vault for MELCOR is 119 kPa and that predicted by the RELAP5/ATHENA model is 129 kPa. The vault pressure in the RELAP5/ATHENA model takes longer to reach equilibrium with the VV than does the MELCOR model. The main reason for the discrepancy is again related to the ability of the models to clear the flow path of coolant so air can flow from the TCWS vault to the

VV. The clearing of the flow path is in turn related to the difference in the inter-phase drag correlation used in the two codes.

The mass flow rate from the VV to the drain tank for both models is shown in Figure 26. The integrated mass flow corresponding to the mass flow rates contained in Figure 26 is shown in Figure 27. The results in Figure 26 show that initially the mass flow rate to the drain tank predicted by the MELCOR model is greater than that from the RELAP5/ATHENA model. The results in Figure 27 show that the total mass flow to the drain tank corresponding to the MELCOR model reaches 40000 kg by 1730 seconds and then gradually increases to 43100 kg at the end of 5000 seconds. The total mass flow to the drain tank from the RELAP5/ATHENA shows the total mass flow reaches 44000 kg by 2660 seconds and then slowly increases to 44150 kg at the end of 5000 seconds. At the end of 5000 seconds 1050 kg more of coolant mass is predicted to flow to the drain tank by the RELAP5/ATHENA model.

The integrated mass flow to the suppression tank for both models is shown in Figure 28. Again the total mass flow for the MELCOR model increases faster, raising from 0.0 to 12700 kg by 1520 seconds and then increasing to 12950 kg at the end of 5000 seconds.   The RELAP5/ATHENA models the total mass flow rising from 0.0 to 15300 kg by 2220 seconds and then increasing to 15400 kg at the end of 5000 seconds thus 2450 kg more of coolant mass is predicted to flow to the suppression tank by the RELAP5/ATHENA model.

In the next two Figures, 29 and 30 we show the air mass flow rate and the integrated mass flow from the in-vessel break to the suppression tank by way of the VV for both models. The MELCOR model predicts that the air in the TCWS vault will commence flowing to the suppression tank at 1200 seconds. The RELAP5/ATHENA model predicts that the flow of air from the vault to the suppression tank will begin at 1650 seconds, a 450 second delay in clearing the flow path between the vault, the VV, and the suppression tank of liquid coolant. Viewing Figure 30 we see that at the end of 5000 seconds the total air mass flow predicted by the RELAP5/ATHENA model is 660 kg vs. 533 kg predicted by the MELCOR model. Although delayed the total air mass from the TCWS vault to the suppression tank is greater by 127 kg for the RELAP5/ATHENA model.

Referring to Figures 22 and 24 we see that the predicted total mass flow to the vault is greater for the MECLOR model, however the vault pressure in Figure 24 predicted by the RELAP5/ATHENA model (129 kPa) is greater than that predicted by the MELCOR model (119 kPa).   This is due to the difference in heat transfer from the vault atmosphere to the vault wall as seen in Figure 31. The difference in heat transfer rate is due to the different heat transfer/steam condensation correlations used in these codes.

4. CONCLUSIONS

As documented in the preceding sections of this report the development of a beryllium dust oxidation model and the development of a RELAP5/ATHENA model of the divertor ex-vessel pipe break accident contained in ITA 81-08 have been completed as well as the other tasks listed in the TA.

Fair agreement was obtained between the RELAP5/ATHENA and MELCOR model results for the divertor ex-vessel accident. The differences being: 1) the break mass flow rates (choked flow) are higher in MELCOR, 2) air enters the VV much slower in the RELAP5/ATHENA model due to differences in the inter-phase correlations used in the models, in particular slug flow in the RELAP5/ATHENA code, and 3) vault pressure in RELAP5/ATHENA results is higher and decays slower due to different heat transfer/steam condensation correlations used in the two codes. The input deck of the final RELAP5/ATHENA model used to generate the results presented in this report is available upon request.

The development of a hydrogen production model for high Be dust inventory was completed and reported in this document. A listing of the dust oxidation functions that are required by MELCOR to analyze hydrogen production from Be dust is contained in Appendix A. The changes made to the MELCOR wet bypass input deck are listed in Appendix C. Code and deck are available for up load to IDM if needed.

The milestones for this ITA were met. However, some of the milestones were not completed on time due to unforeseen higher priorities associated with ITER, such as the pedigreeing of the fusion version of the MELCOR 1.8.2 code needed to analyze the postulated accidents required for the RPrS review [28] and the verification of the computer inputs deck used in the analyses of the postulated accidents [29].

5. REFERENCES

1. ITER Implementing Task Agreement, "Support and assistance for the latest fusion versions of computer codes," ITA 81-08, extension G 81 TD 21 FU, January (2005).
2. R. L. Moore, "Status Report on an ITER ITA on Comparison of MELCOR 1.8.5 Results to MELCOR 1.8.2 Result for a Selected Set of Accident Analysis Cases Relevant to ITER FEAT," INEEL EDF-5470, January (2005).
3. B. J. Merrill, and R. L. Moore, "Status Report on Code Safety ITER Implementing Task Agreement for Calendar Year 2005," INL-EDF-6607, January (2006).
4. J. R. Welty, C. E. Wicks, and R. E. Wilson, *Fundamentals of Momentum, Heat and Mass Transfer*, John Wiley & Sons, Inc., New York, 1969, p 495.
5. B. Na, and D. L. Webb, "New Model for Frost Growth Rate," International Journal of Heat and Mass Transfer, 47 (2004), p. 925-936.
6. R. A. Anderl, R. J. Pawelko, "Steam Chemical Reactivity of Beryllium Powder," INEEL/EXT-99-00338, April 30, 1999.
7. K. A. McCarthy, et al., "The Safety Implications of Tokamak Dust Size and Surface Area," Fusion Engineering and Design, 42, 1998, p. 45-52.
8. ITER, "Safety Analysis Data List," G 81 RI 10 03-08-08 W 0.1, Version: 4.0.3 SADL, September 26, (2003)
9. F. P. Incropera, and D. P. DeWitt, *Fundamentals of Heat and Mass Transfer (3rd Edition)*, John Wiley & Sons, Inc., New York, 1981, p. 903.
10. J. R. Welty, C. E. Wicks, and R. E. Wilson, *Fundamentals of Momentum, Heat and Mass Transfer*, John Wiley & Sons, Inc., New York, 1969, p. 457.
11. Private communication by email with ITER IT ITA task officer Leonid Topilski, July 26, 2005.
12. G. Smolik et al., "Reaction of porous Beryllium in Steam", INEEL, EGG-FSP-10346, July 1992.
13. R. A. Anderl, et al.,"Steam-chemical reactivity for irradiated beryllium," Journal of Nuclear Materials, 258-263 (1998), p. 750-756.
14. H. Niessen, and S. Ball (editors), *Heat Transport and Afterheat Removal for Gas Cooled Reactors Under Accident Conditions*, International Atomic Energy Agency, IAEA-TECDOC-1163.
15. P. Zehner, and E. U. Schlünder, "Thermal Conductivity of Granular Material at Moderate Temperatures," *Chemie-Ingr-Tech*, 42, pp933-941, 1970. In German.
16. G. Breitbach, and H. Barthels, "The Radiant Heat Transfer in the HTR Core After Failure of the Afterheat Removal Systems," *Nuclear Technology*, 49, pp392-399, August 1980.
17. V. Prasad, N. Kladas, A. Bandyopadhaya and Q. Tian, "Evaluation of Correlations for Stagnant Thermal Conductivity of Liquid-Saturated Porous Beds of Spheres," *International Journal of Heat and Mass Transfer*, 32, p. 1783-1796 (1989).
18. Mathcad 11 User's Guide, Mathsoft Engineering & Education, Inc. Cambridge, MA.
19. C. A. Meyer, *1967 ASME Steam Tables Thermodynamic and Transport Properties of Steam Comprising Tables and Charts for Steam and Water*, American Society of Mechanical Engineers; 2nd edition (January 1, 1968).
20. ITER, ""Generic Site Safety Report: Volume VII Appendix A," G 84 RI 6 01-07-10 R 1.0, July (2004), p. VII 267-292.
21. ITER, "Safety Analysis Data List," ITER_D_24LSAE, Version: 5.2 SADL, September 5, (2007), p. 12.
22. S. Song, and M. M. Yovanovich, "Thermal Gap Conductance: Effects of Gas Pressure and Mechanical Load," *Journal of Thermophysics and Heat Transfer*, Vol. 6, No 1, p. 62-68 (1992).

23. W. Cheng, and C. Madhusudana, "Decrease in Thermal Contact Conductance and the Contact Pressure of Finned-Tube Heat Exchangers Assembled with Different Sixe Bullets," *Journal of Heat Transfer*, 129, July (2007), p. 907-911.
24. J. R. Welty, C. E. Wicks, and R. E. Wilson, *Fundamentals of Momentum, Heat and Mass Transfer*, John Wiley & Sons, Inc., New York, 1969, p. 215.
25. M. Shapiro, et al., "Characterization of Powder Beds by Thermal Conductivity: Effect of Gas Pressure on the Thermal Resistance of Particle Contact Points," *Particle & Particle Systems Characterization*, 21 (2004), p. 268-275.
26. ITER, "Accident Analysis Specification," ITER_D_258QGE, Version 2.5, November 30, 2007.
27. Symbolic Nuclear Analysis Package 0.27.2 (Pre-Release) March 06, 2008, Applied Programming Technology, Inc.
28. R. L. Moore, "Pedigree Analysis of the MELCOR 1.8.2 Code to be Used for ITER's Report Preliminary on Safety," INL/EXT-07-12856, June (2007).
29. R. L. Moore, "Verification of MELCOR Input Decks Used in ITER RPrS Analyses," INL/EXT-07-13305, January (2008).
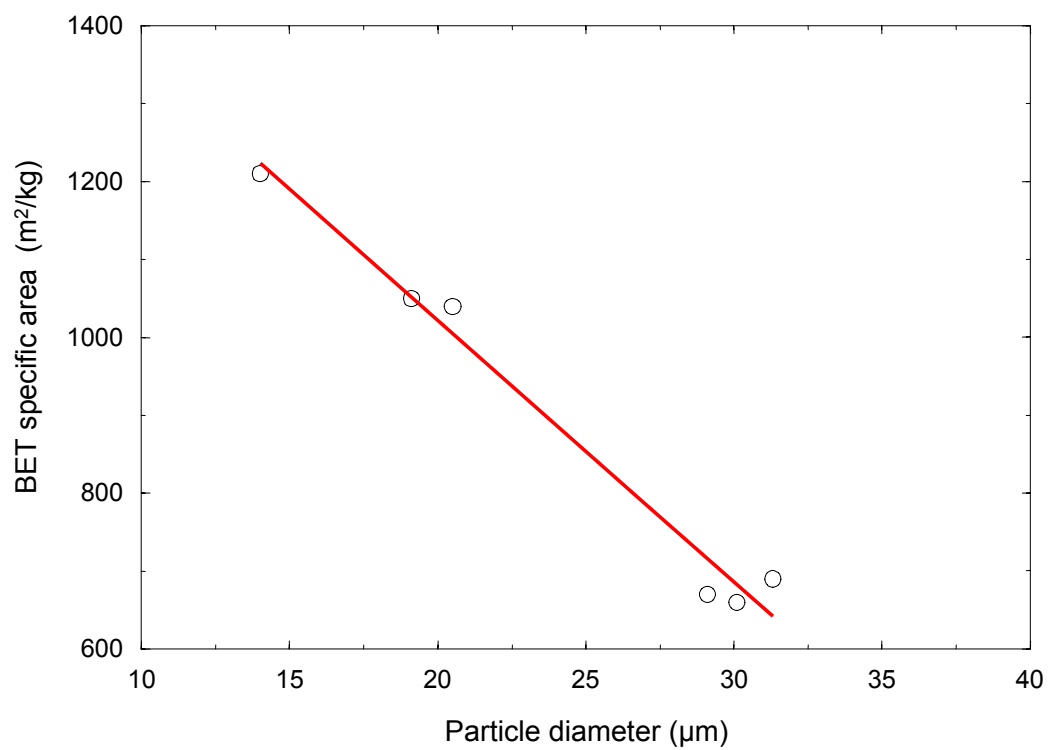
Figure 1. Comparison of INL BET measured specific surface area for beryllium dust to the predictions for Equation 4.
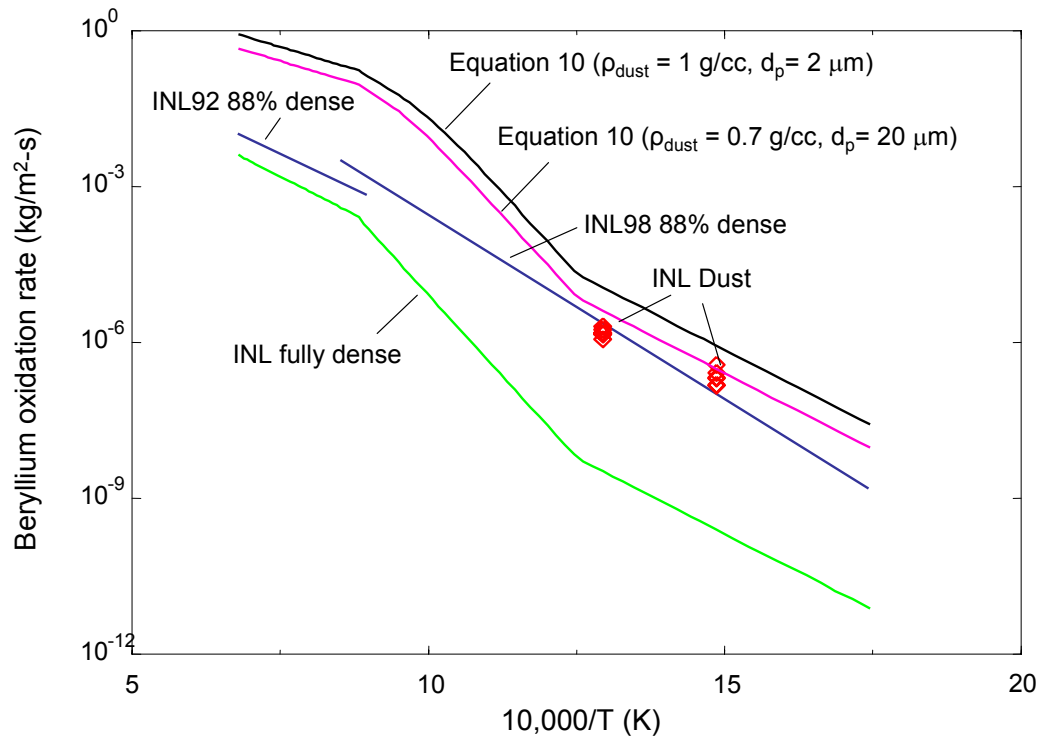
Figure 2. Comparison of INL beryllium-steam oxidation rate equations based on the test specimen geometric surface area with the predictions of Equation 10.
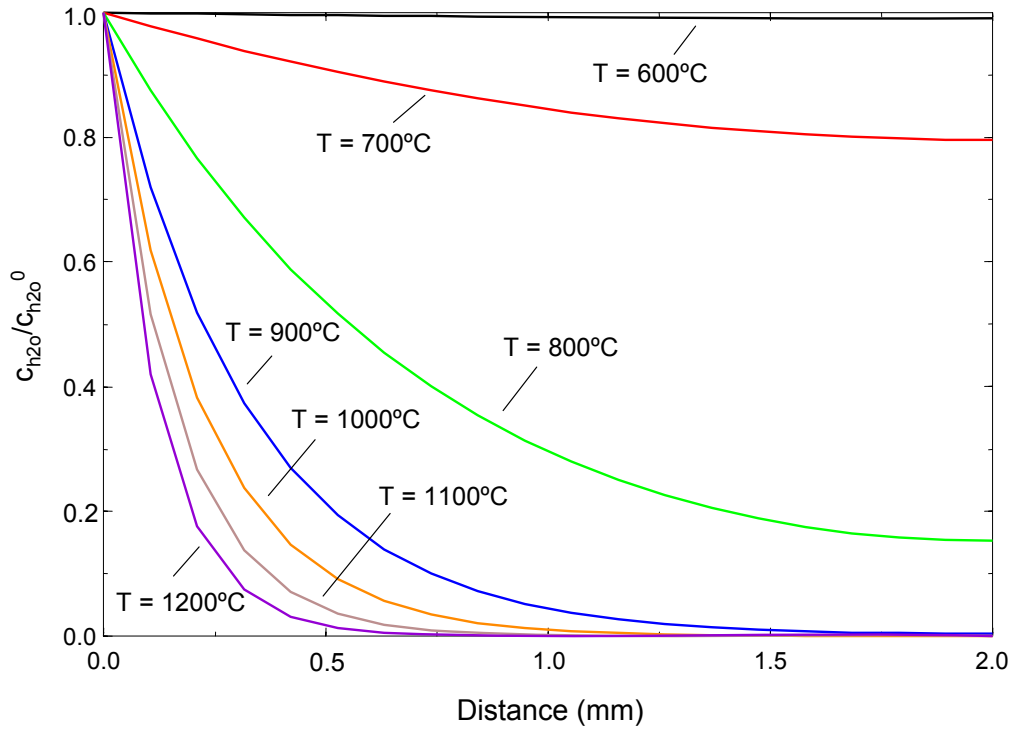
Figure 3. Relative steam concentration in a 2 mm beryllium layer at various layer temperatures as predicted by Equation 9.
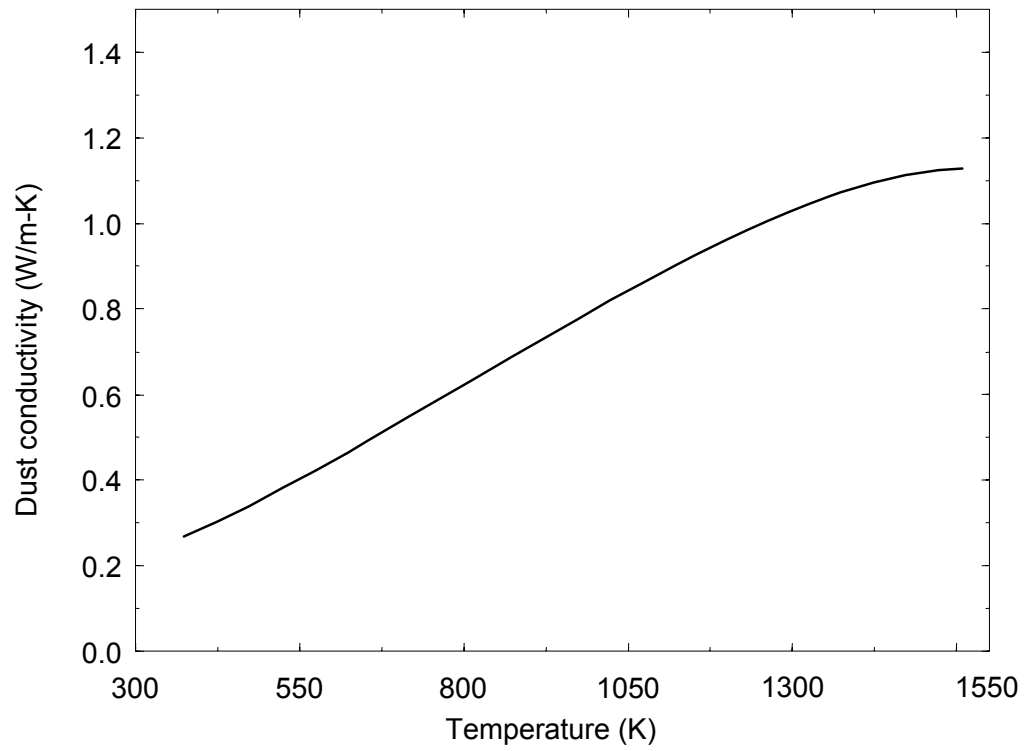
Figure 4. Beryllium dust layer effective thermal conductivity based on Equation 19.
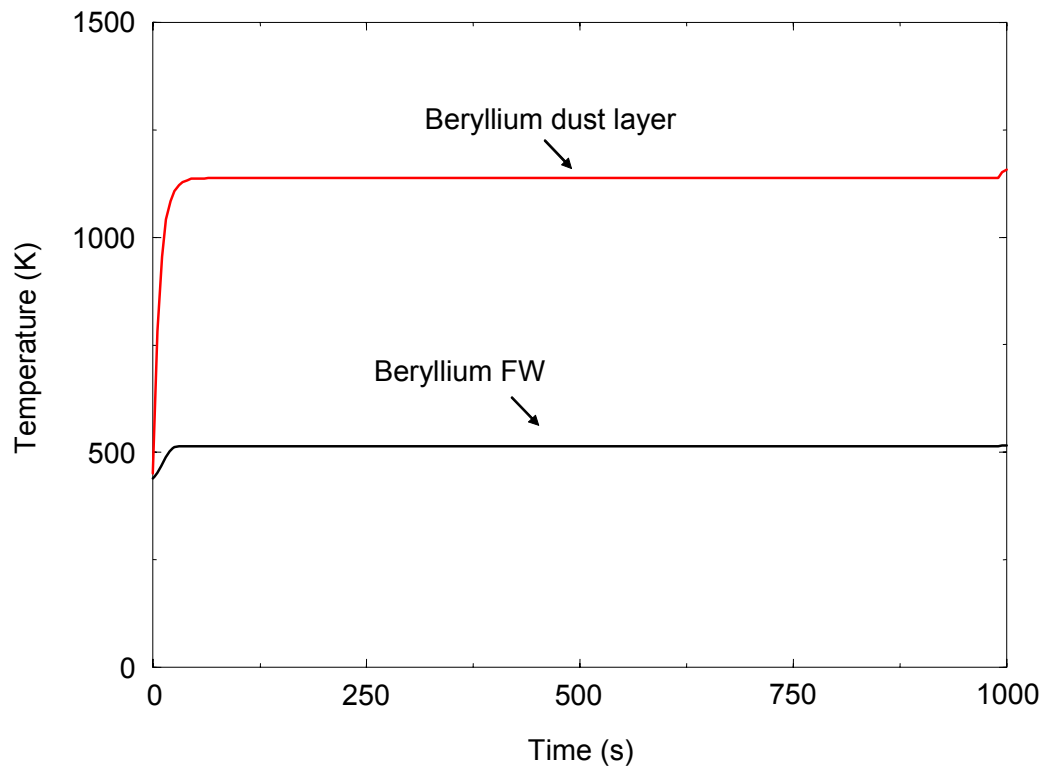
Figure 5. Inboard first wall surface temperature comparison with and without a beryllium dust layer during normal operating conditions.
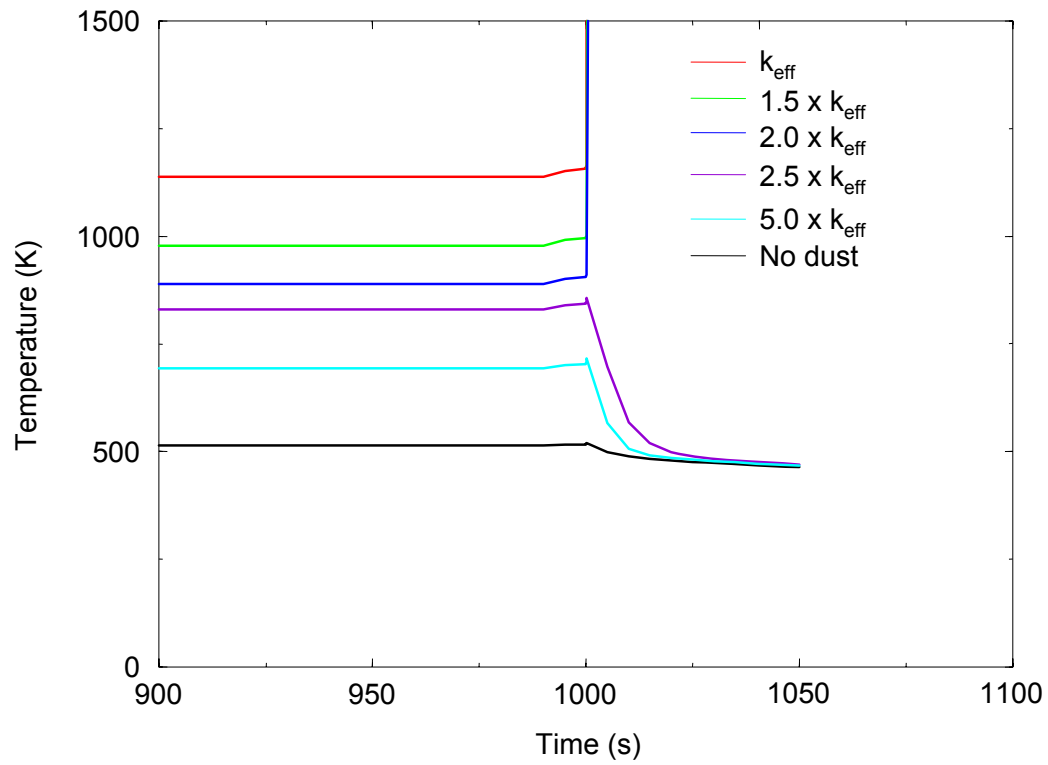
Figure 6. Inboard first wall surface temperature comparison with differing beryllium dust layer effective thermal conductivity during an in-vessel steam loss-of-coolant accident.

Fig. 3 Gap-conductance results of experiment 1.
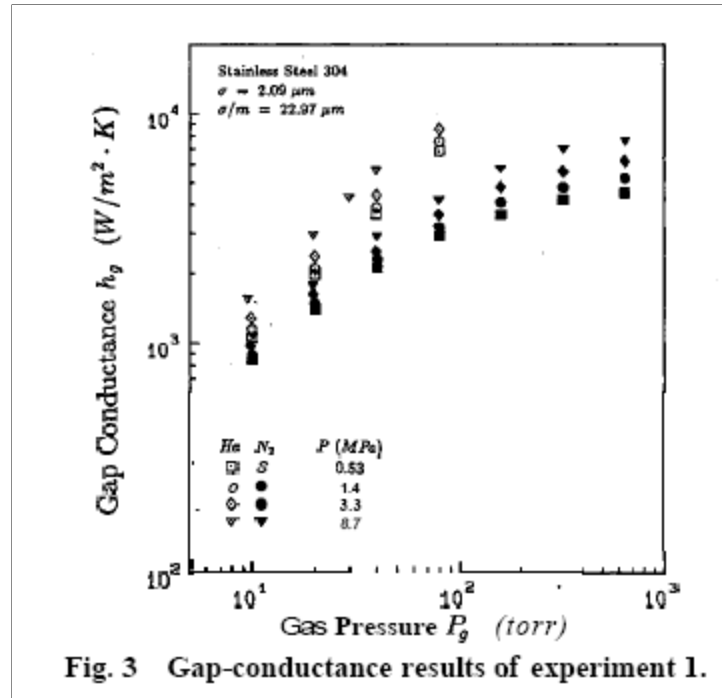
Figure 7. Measure variation of gap conductance with gas pressure and mechanical load in experiment 1 of Reference 22.
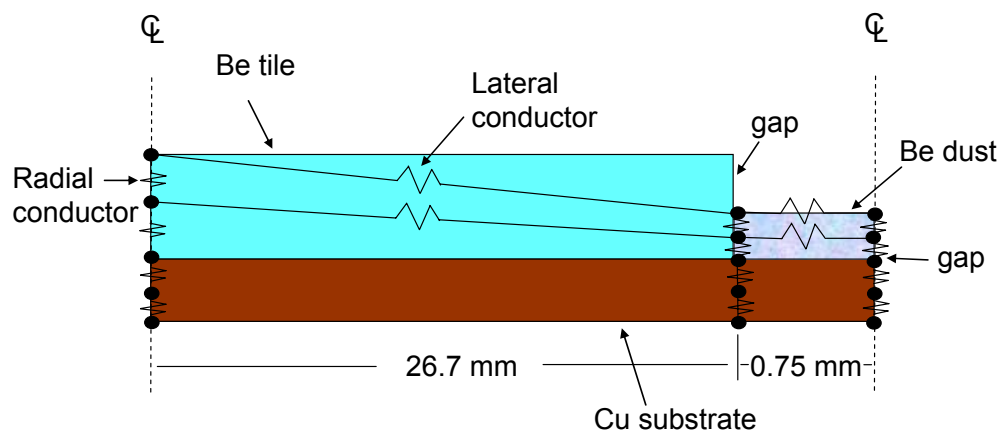
Figure 8. Schematic of MELCOR 2D dust heat conduction model.
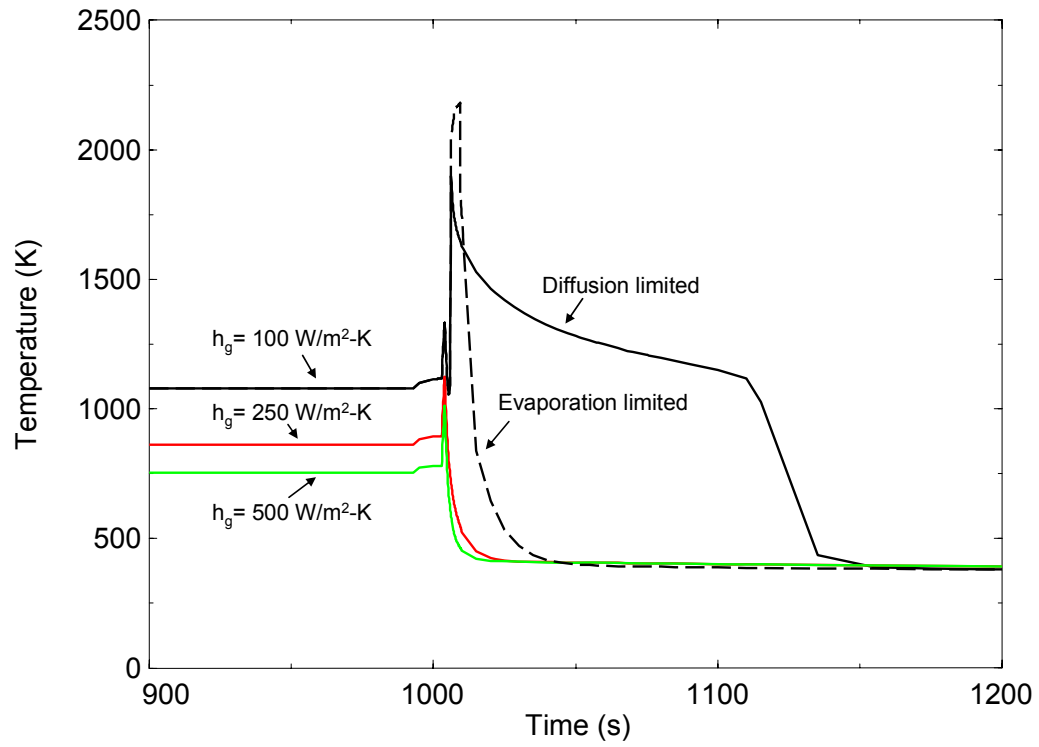
Figure 9. Dust surface temperature during a wet bypass accident for different dust to tile gap conductances.
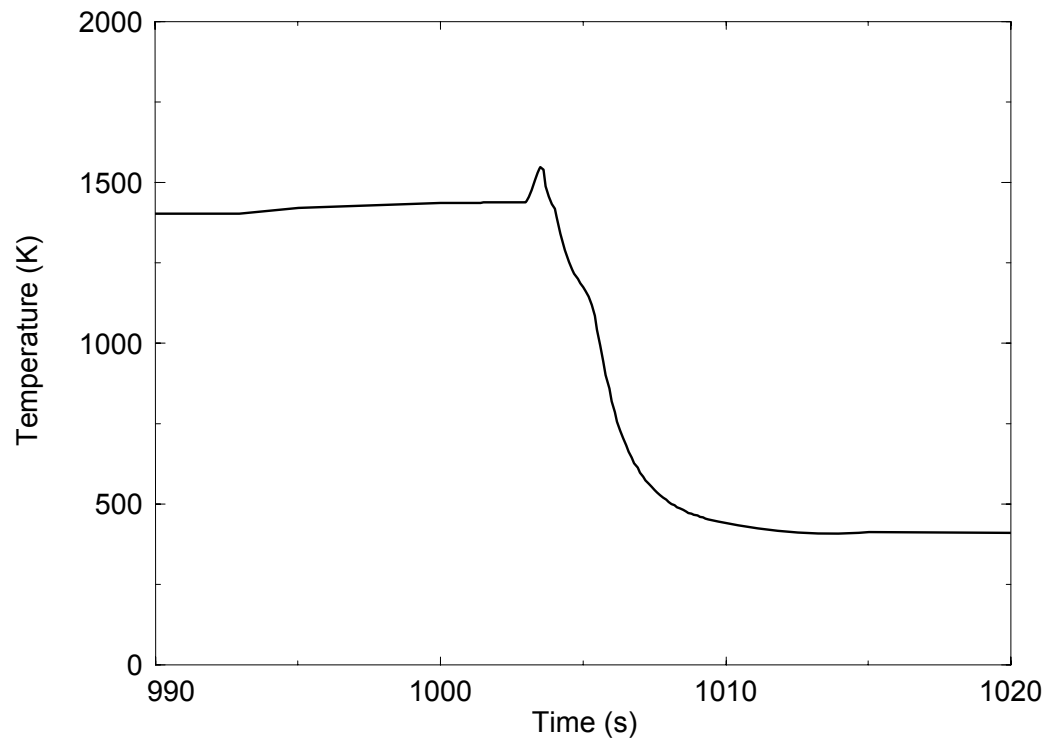
Figure 10. Dust surface temperature during a wet bypass accident when Equation 20 is used to predict dust to tile gap conductance.
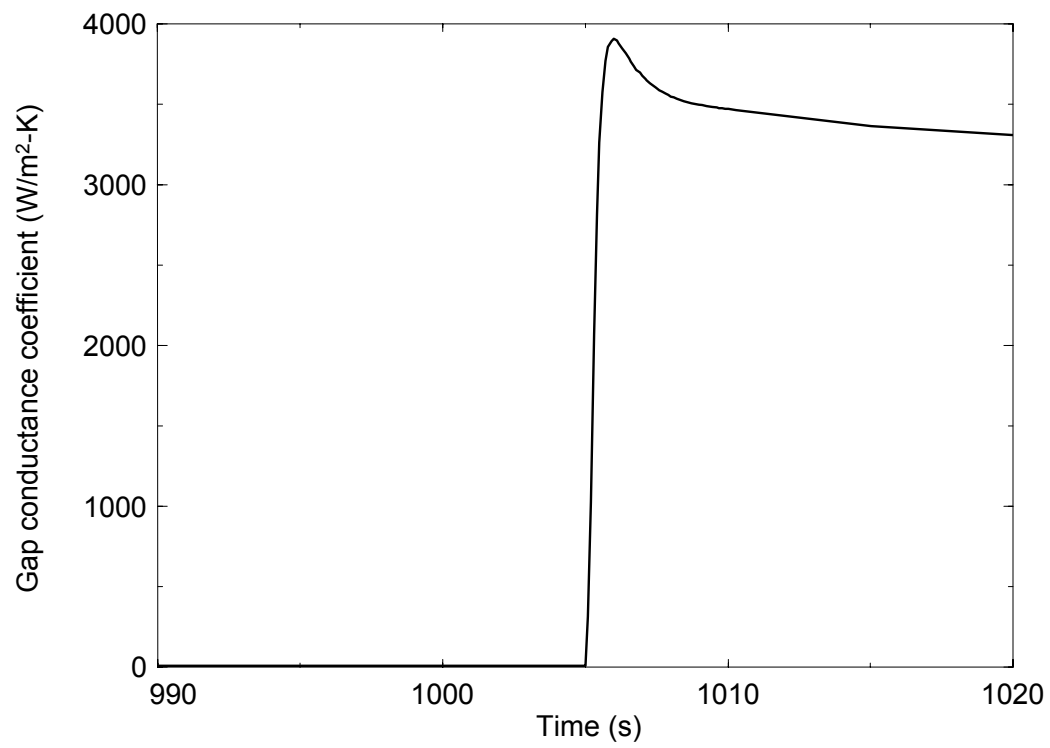
Figure 11. Dust to tile gap conductance during a wet bypass accident when Equation 20 is used to predict gap conductance.
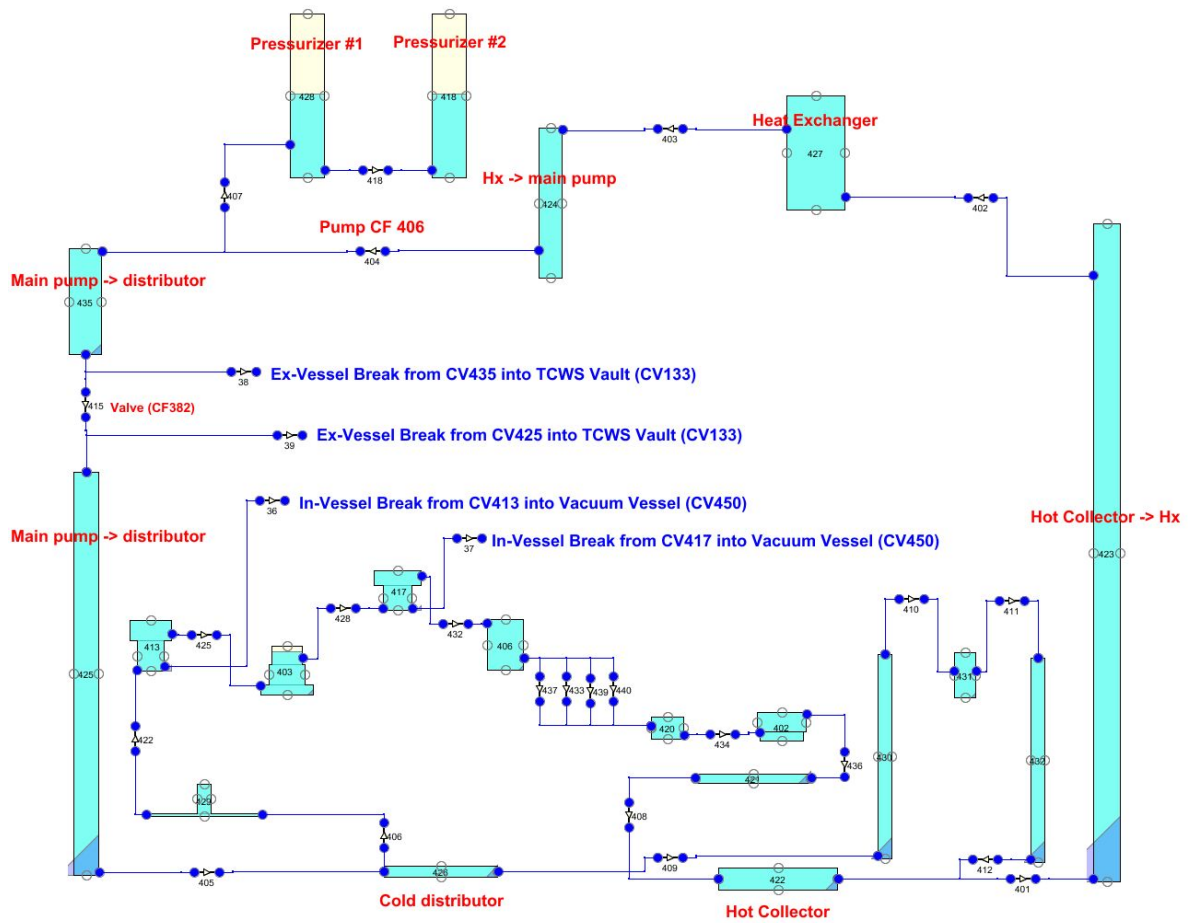
Figure 12. Schematic of the MELCOR Divertor Loop Model as represented in the feat2004.divsimpf.inp computer deck.
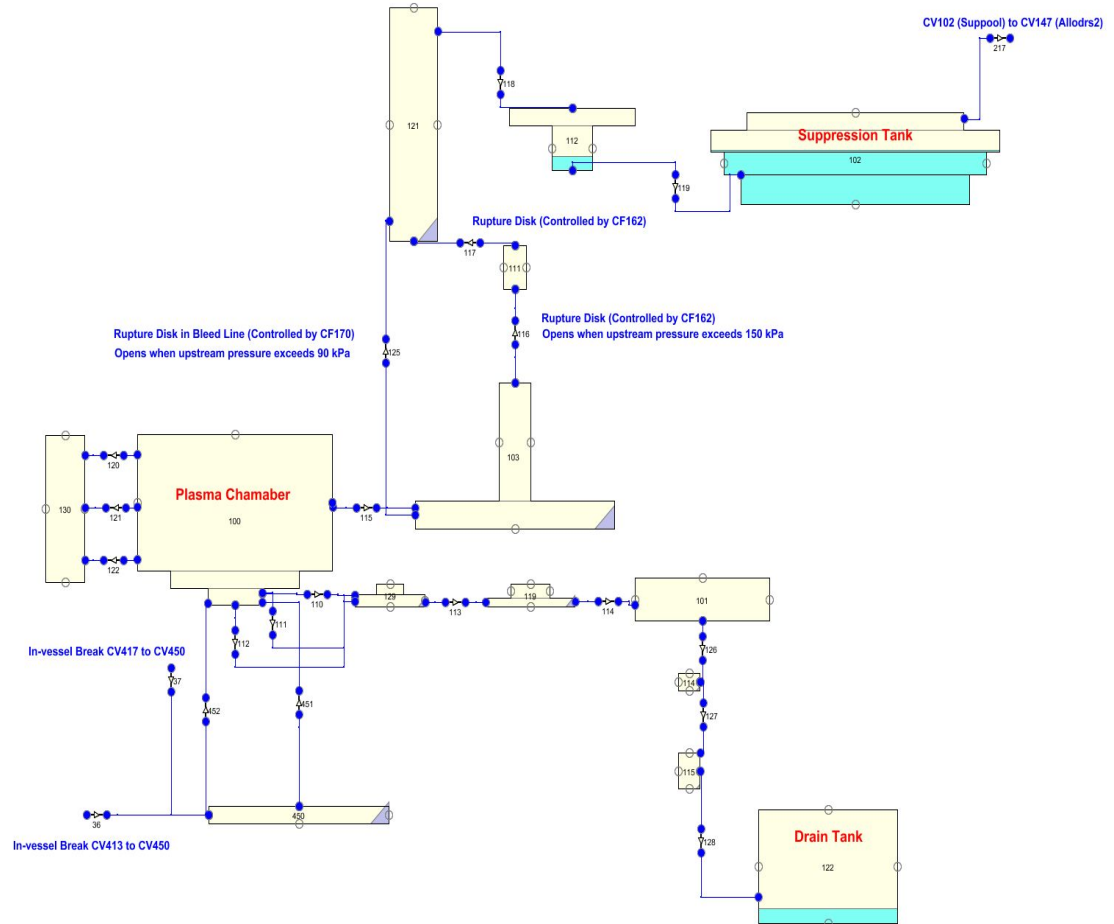
Figure 13. Schematic of the MELCOR Suppression System Model as represented in the feat2004.divsimpf.inp computer deck.
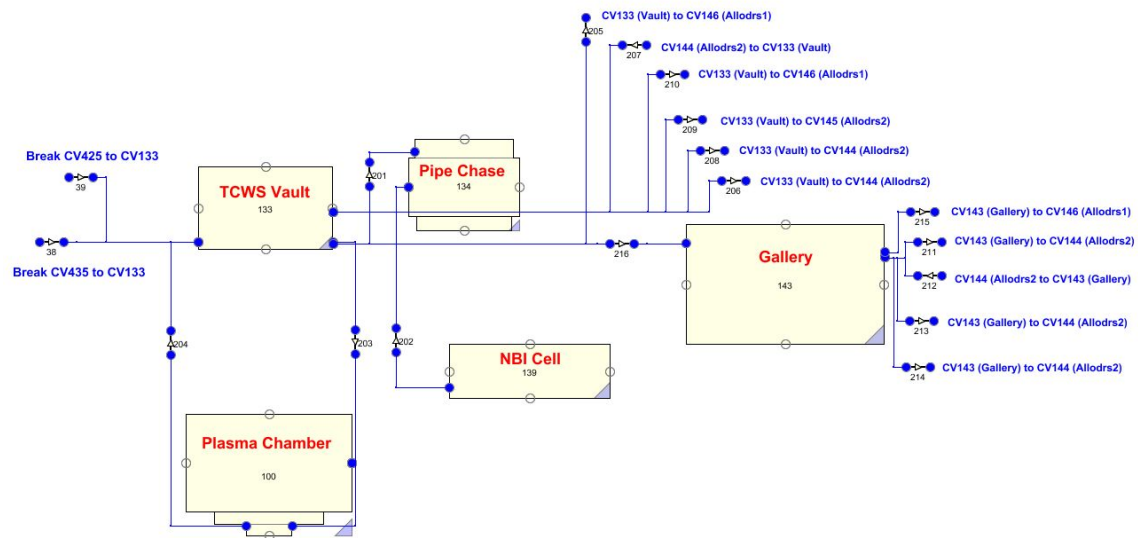
Figure 14. Schematic of the MELCOR Vault System Model as represented in the feat2004.divsimpf.inp computer deck.
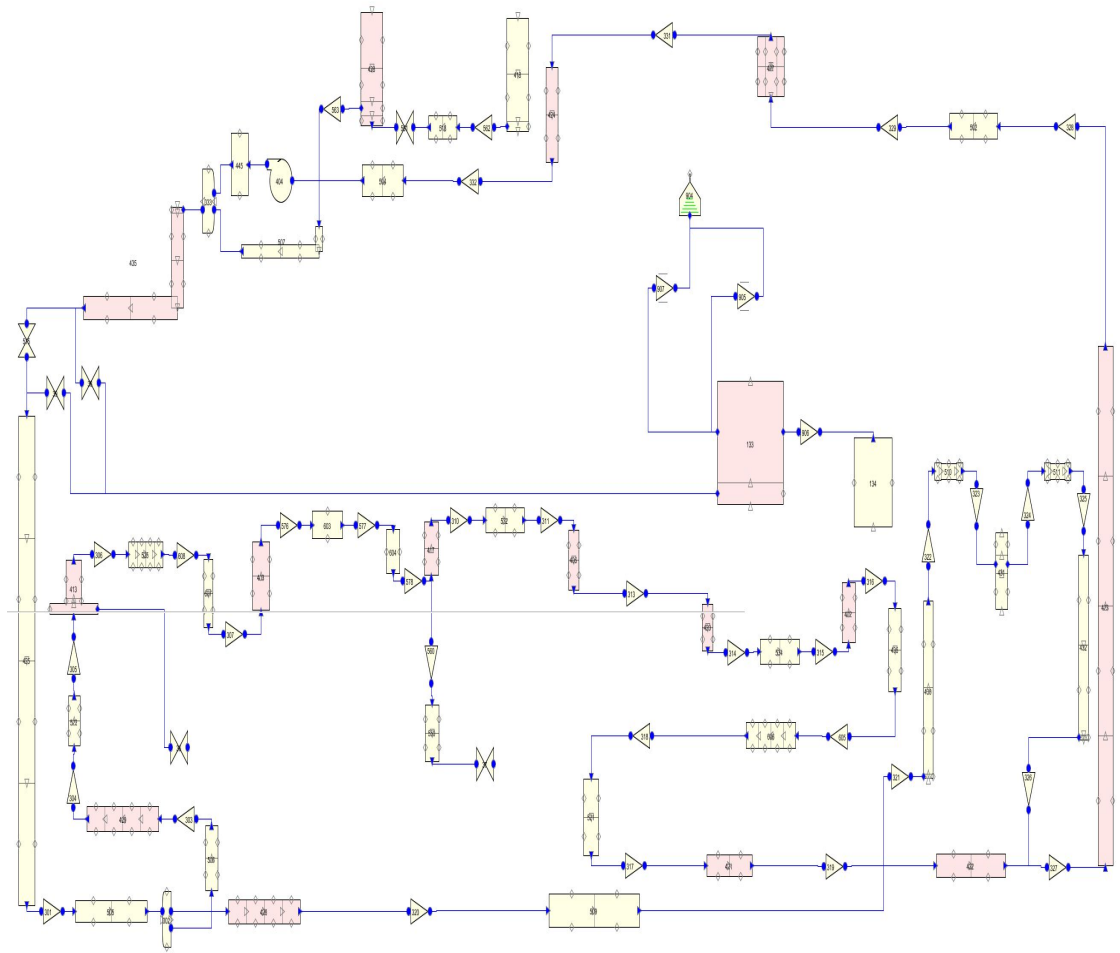
Figure 15. Schematic of the RELAP5/ATHENA Divertor Loop Model.
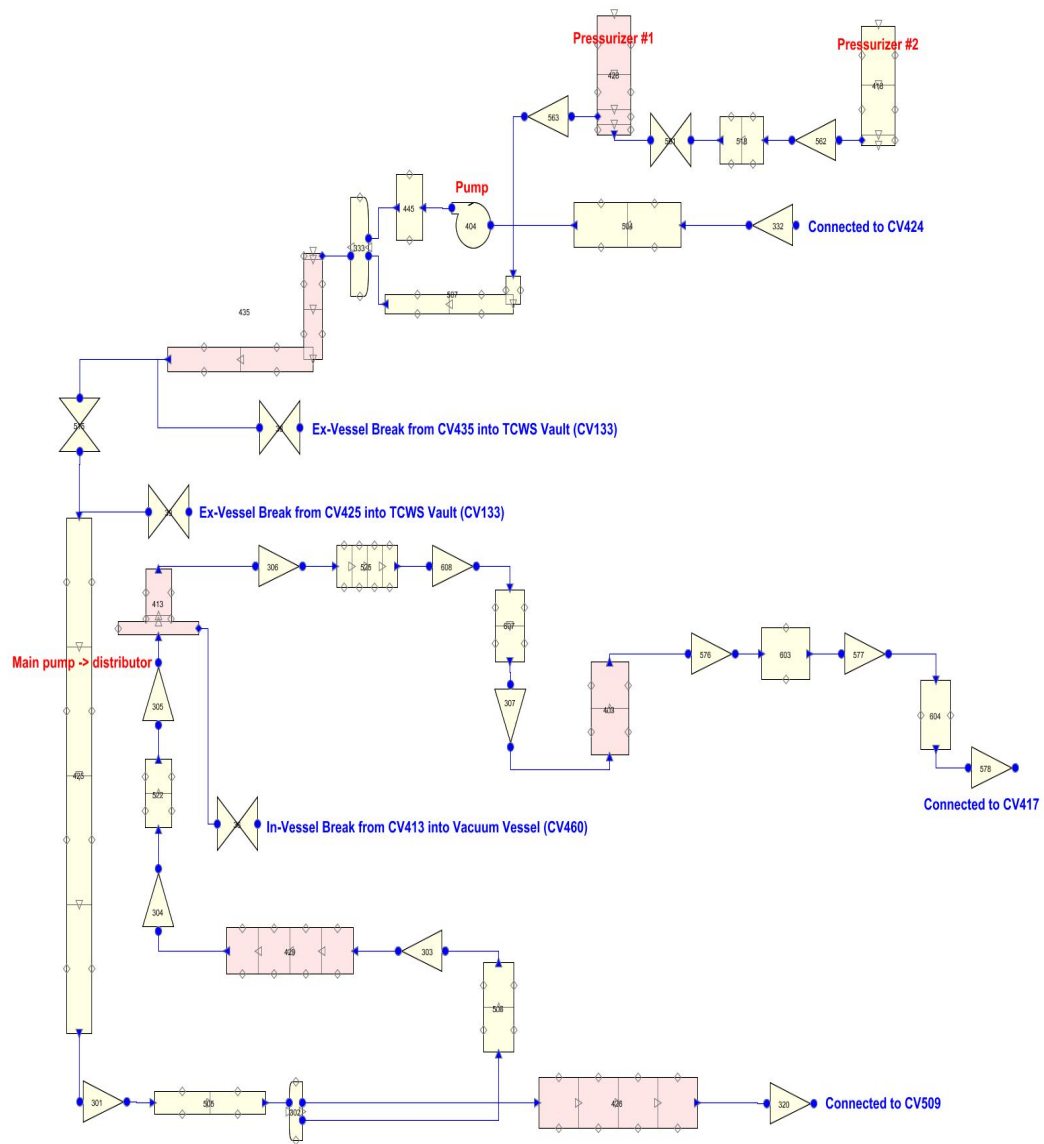
Figure 16. Schematic of the left side of the RELAP5/ATHENA Divertor Loop Model.
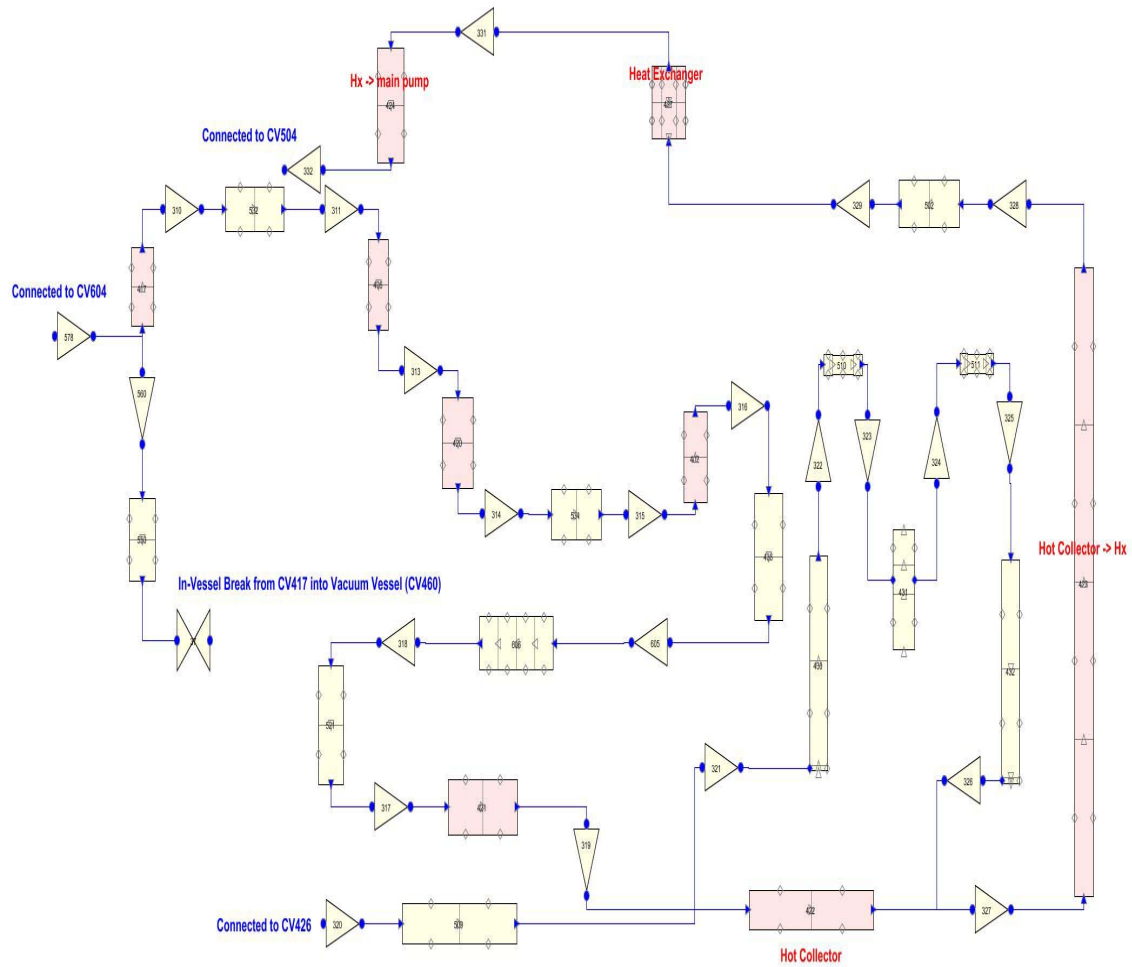
Figure 17. Schematic of the right side of the RELAP5/ATHENA Divertor Loop Model.
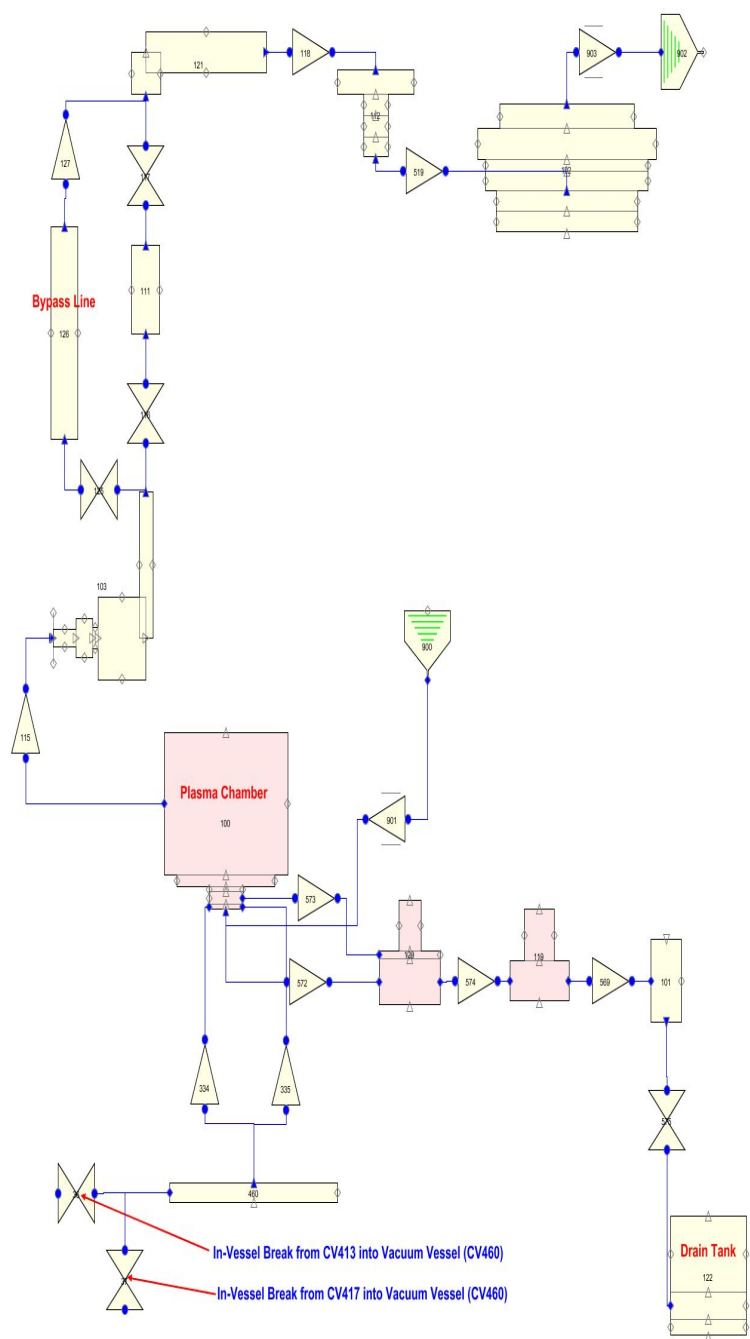
Figure 18. Schematic of the RELAP5/ATHENA Suppression System Model.

Bypass Line

Plasma Chamber

In-Vessel Break from CV413 into Vacuum Vessel (CV460)

In-Vessel Break from CV417 into Vacuum Vessel (CV460)

Drain Tank
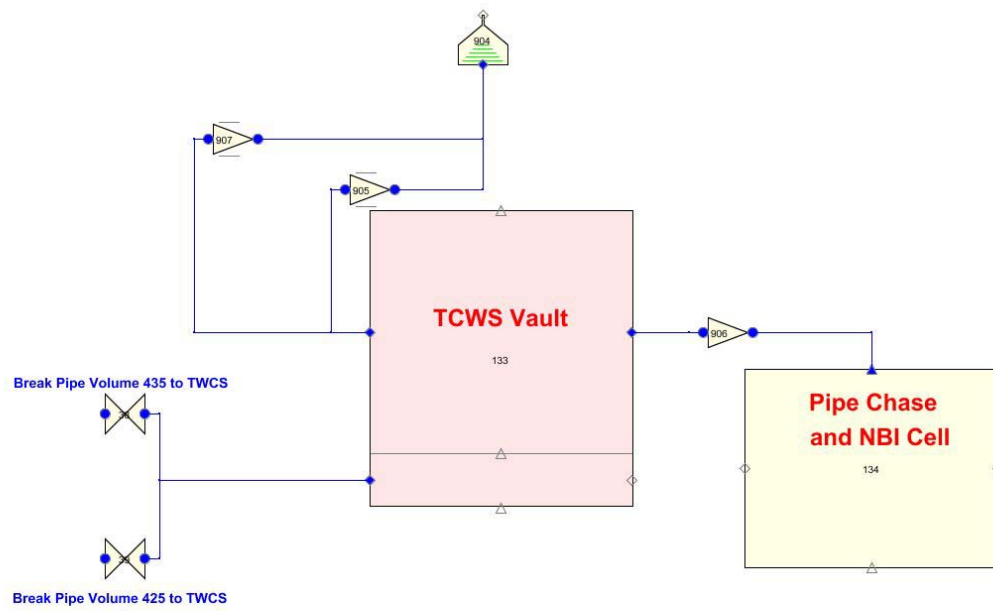
Figure 19. Schematic of the RELAP5/ATHENA Vault System Model.
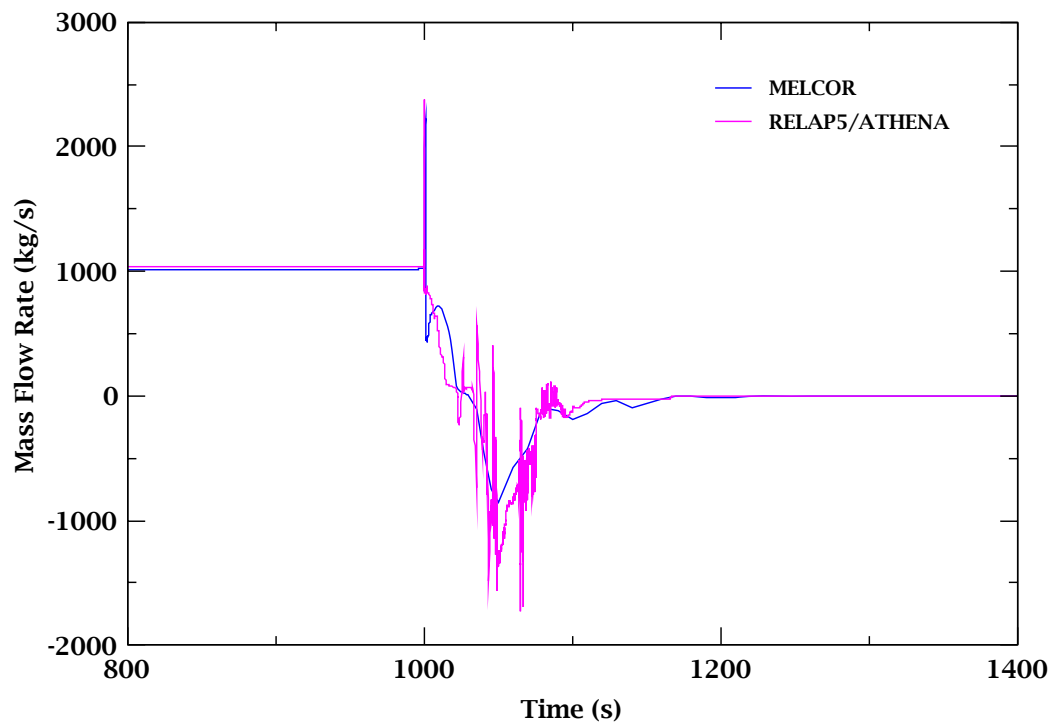
Figure 20. Comparison of the MELCOR and RELAP5/ATHENA total loop mass flow rates.
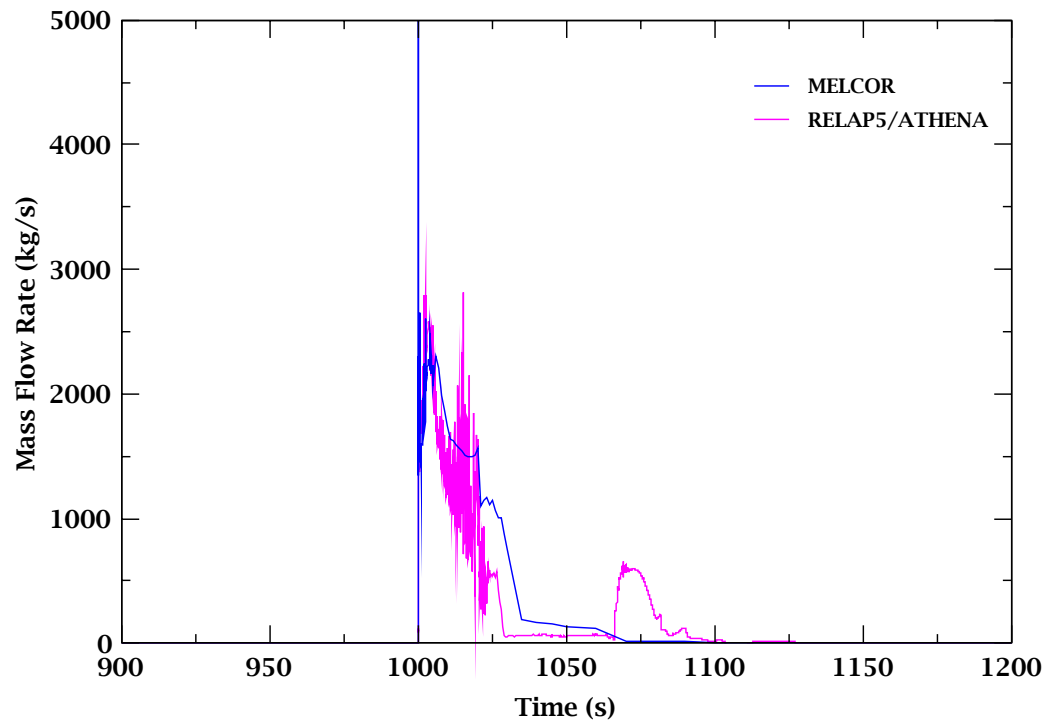
Figure 21. Comparison of the MELCOR and RELAP5/ATHENA mass flow from the ex-vessel break to the TCWS vault.
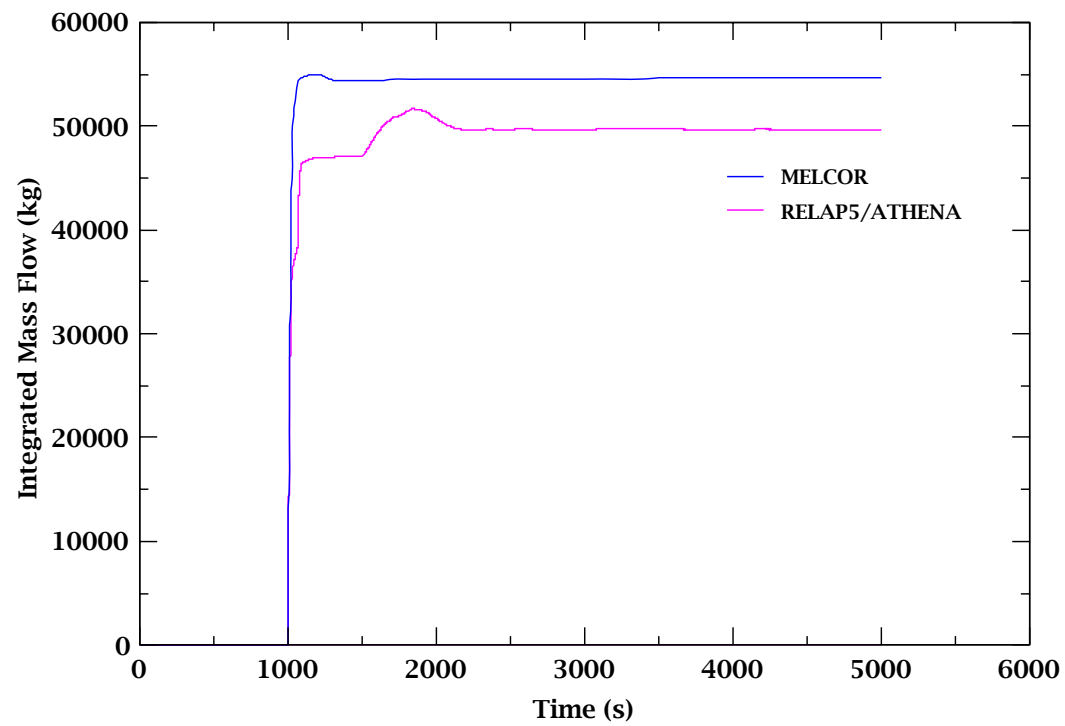
Figure 22. Comparison of the MELCOR and RELAP5/ATHENA integrated mass flow from the ex-vessel break to TCWS vault.
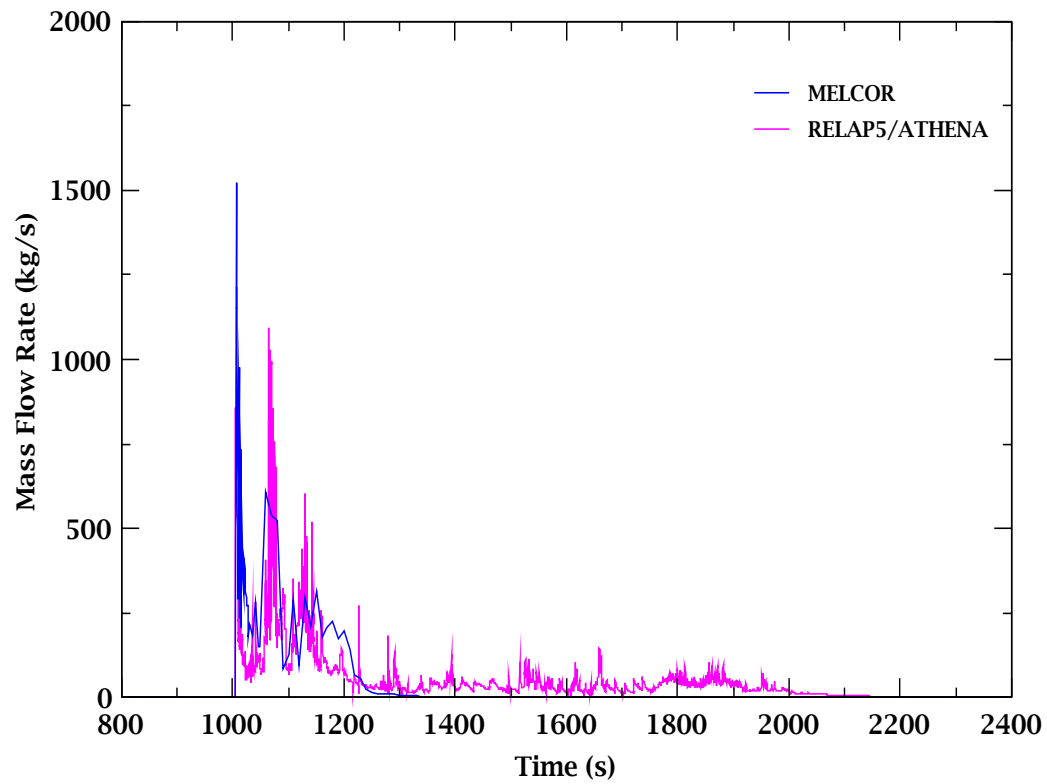
Figure 23. Comparison of MELCOR and RELAP5/ATHENA in-vessel break mass flow rates.
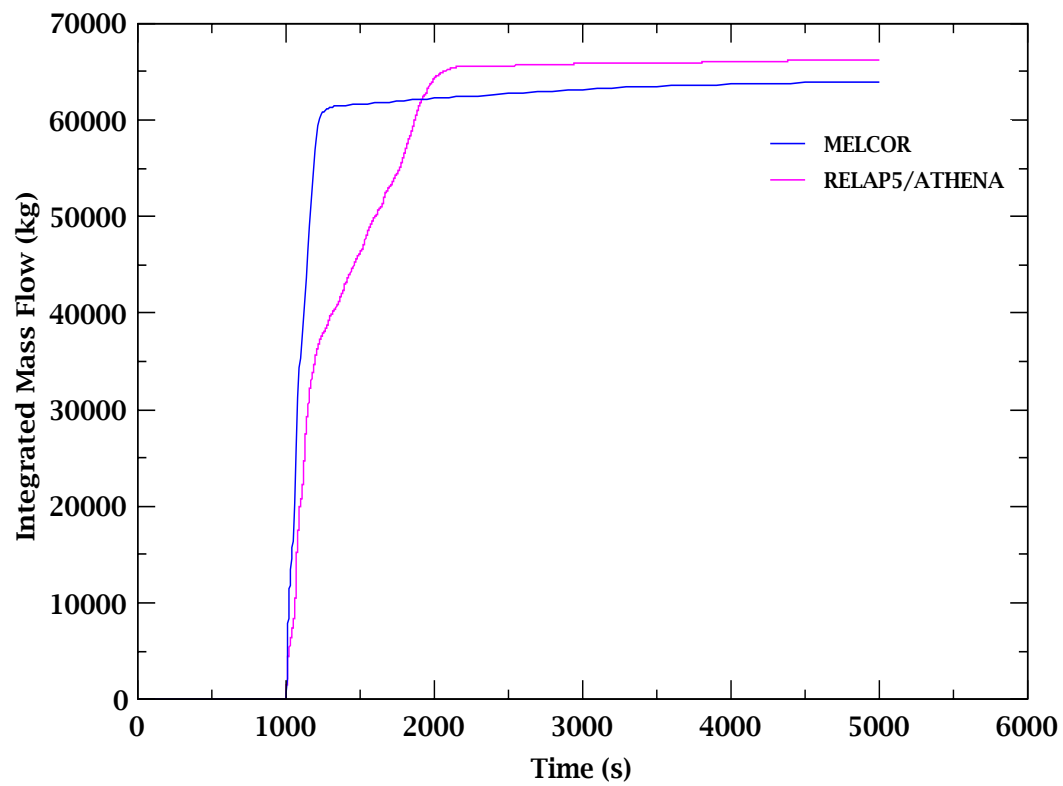
Figure 24. Comparison of the MELCOR and RELAP5/ATHENA integrated mass flow from the in-vessel break to the vacuum vessel.
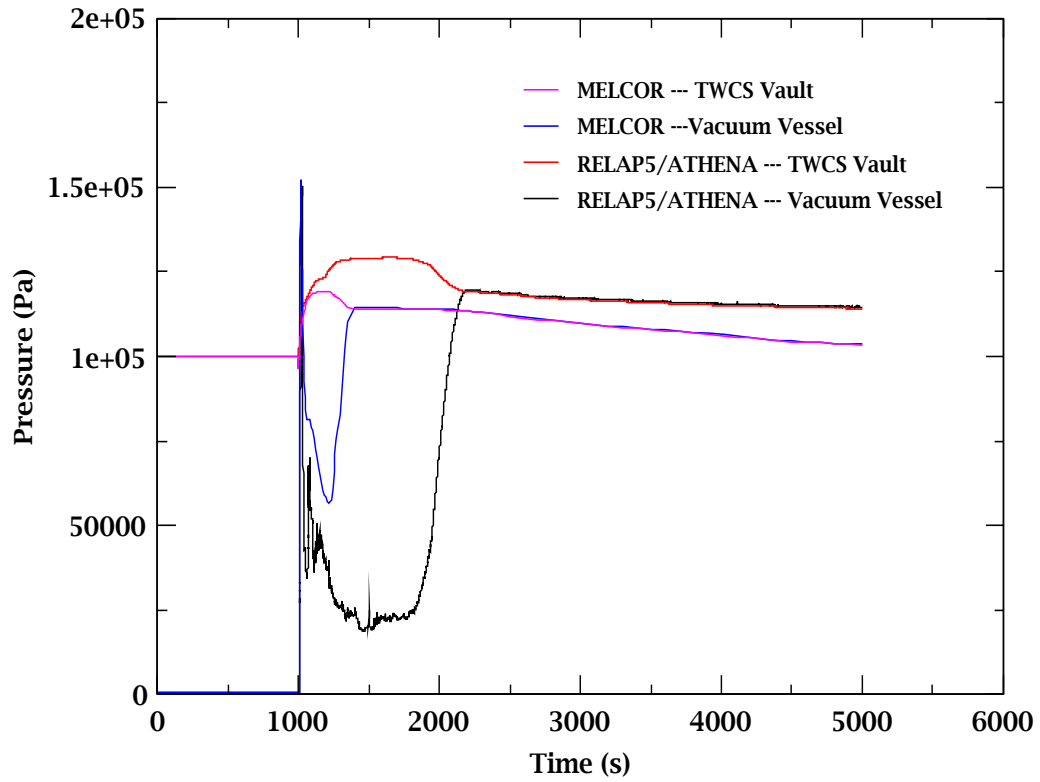
Figure 25. Comparison of the MELCOR and RELAP5/ATHENA pressure histories in the TCWS vault and the vacuum vessel.
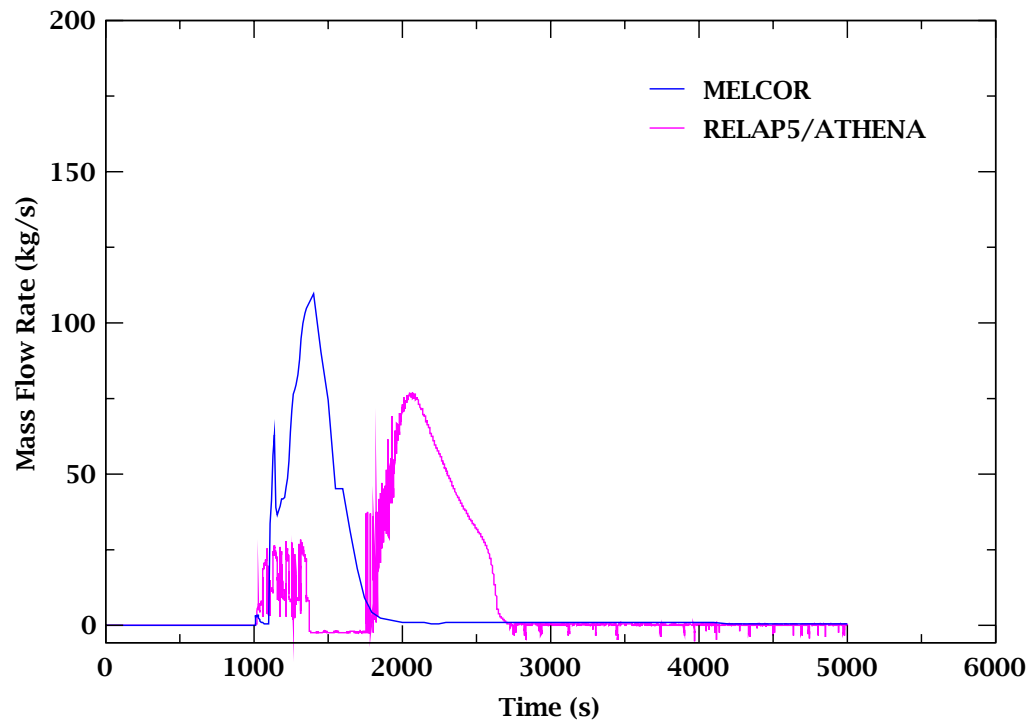
Figure 26. Comparison of the MELCOR and RELAP5/ATHENA mass flow from the vacuum vessel to the drain tank.
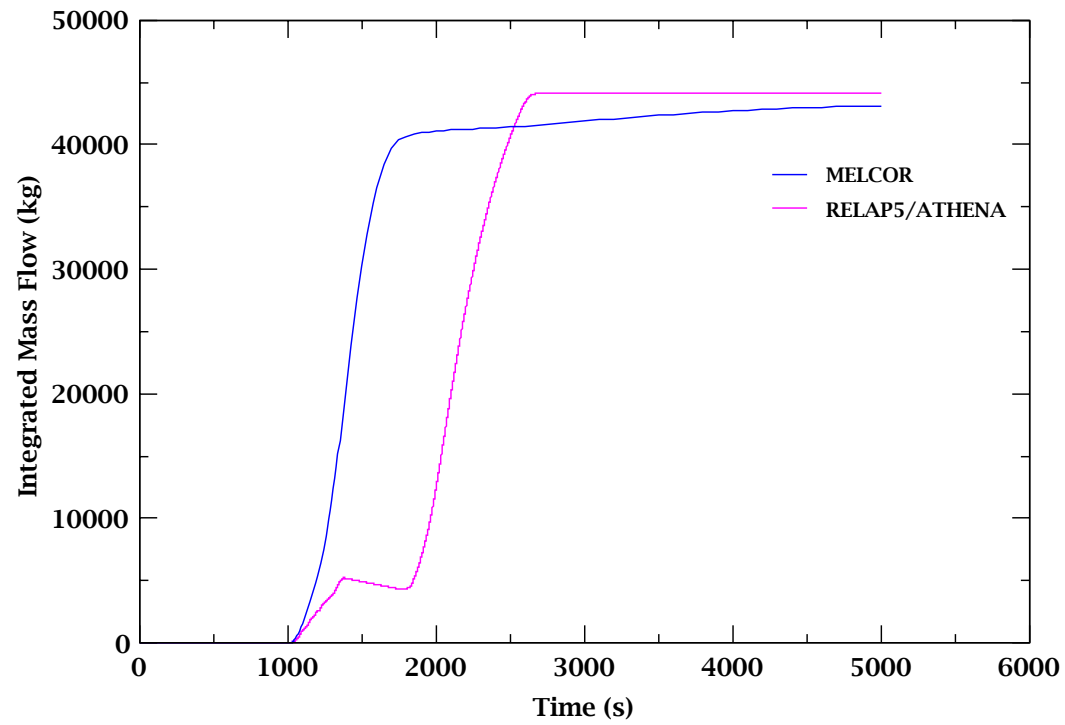
Figure 27. Comparison of the MELCOR and RELAP5/ATHENA integrated mass flow from the vacuum vessel to the drain tank.
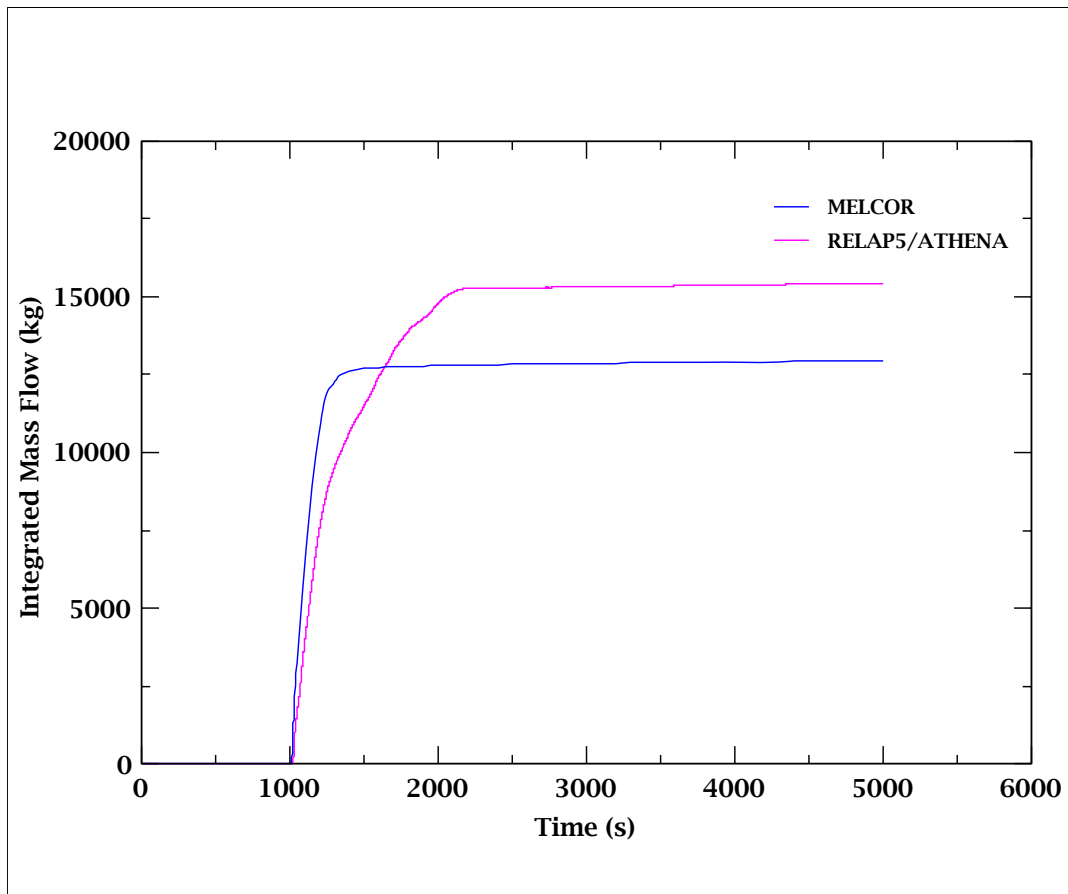
Figure 28. Comparison of the MELCOR and RELAP5/ATHENA integrated mass flow from the vacuum vessel to the suppression tank.
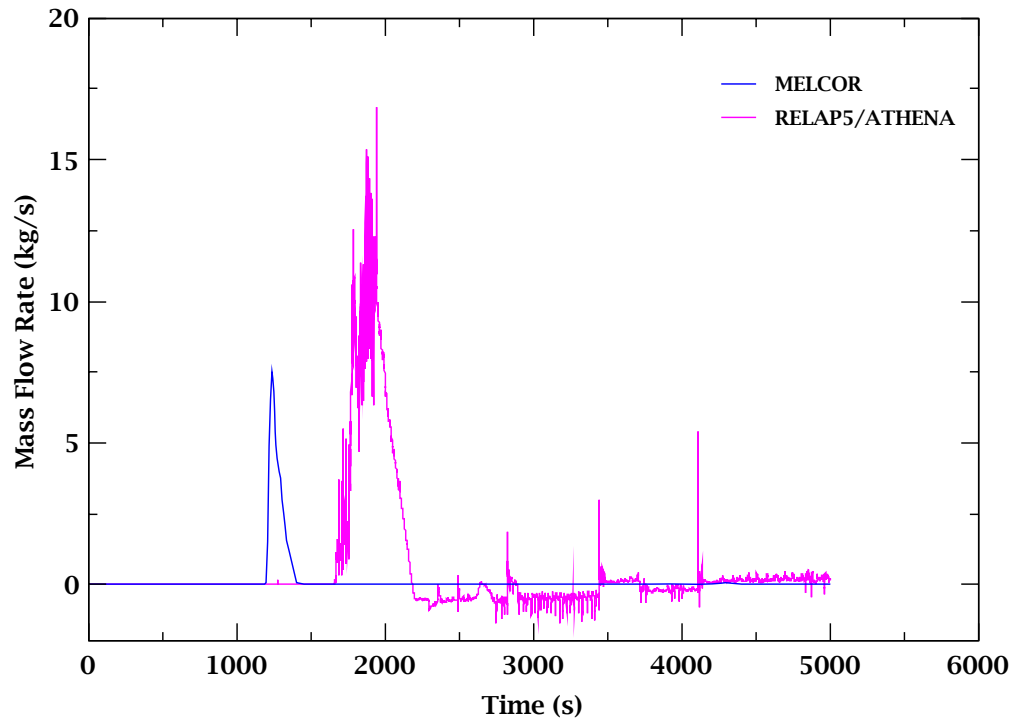
Figure 29. Comparison of the MELCOR and RELAP5/ATHENA air mass flow from the in-vessel break to the vacuum vessel.
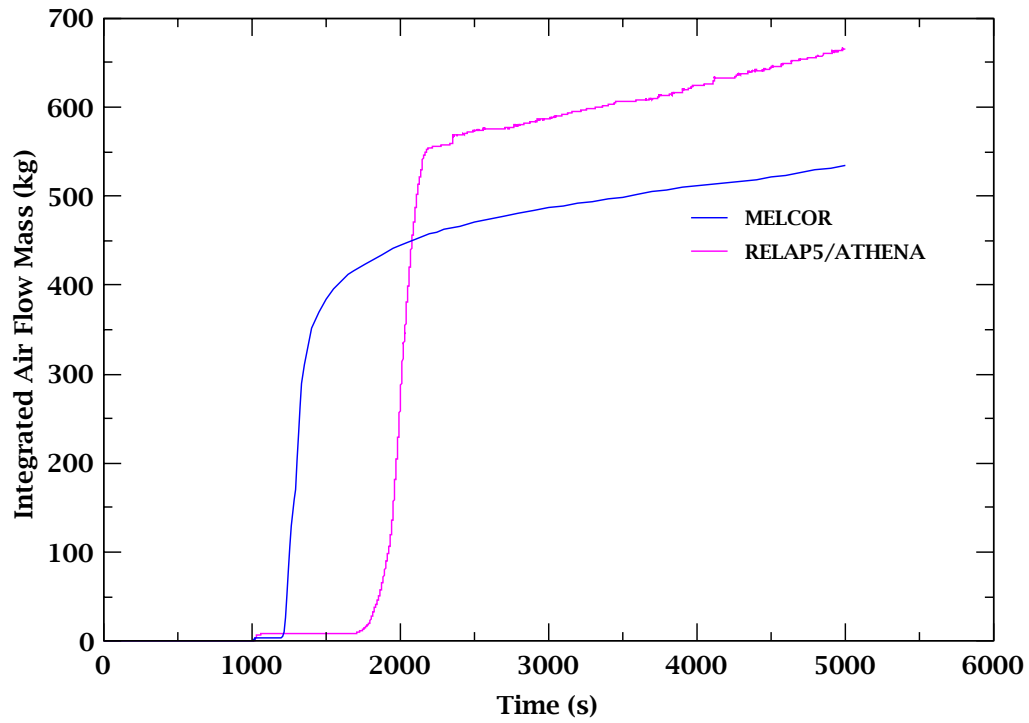
Figure 30. Comparison of the MELCOR and RELAP5/ATHENA integrated air mass flow from the vacuum vessel to the suppression tank.
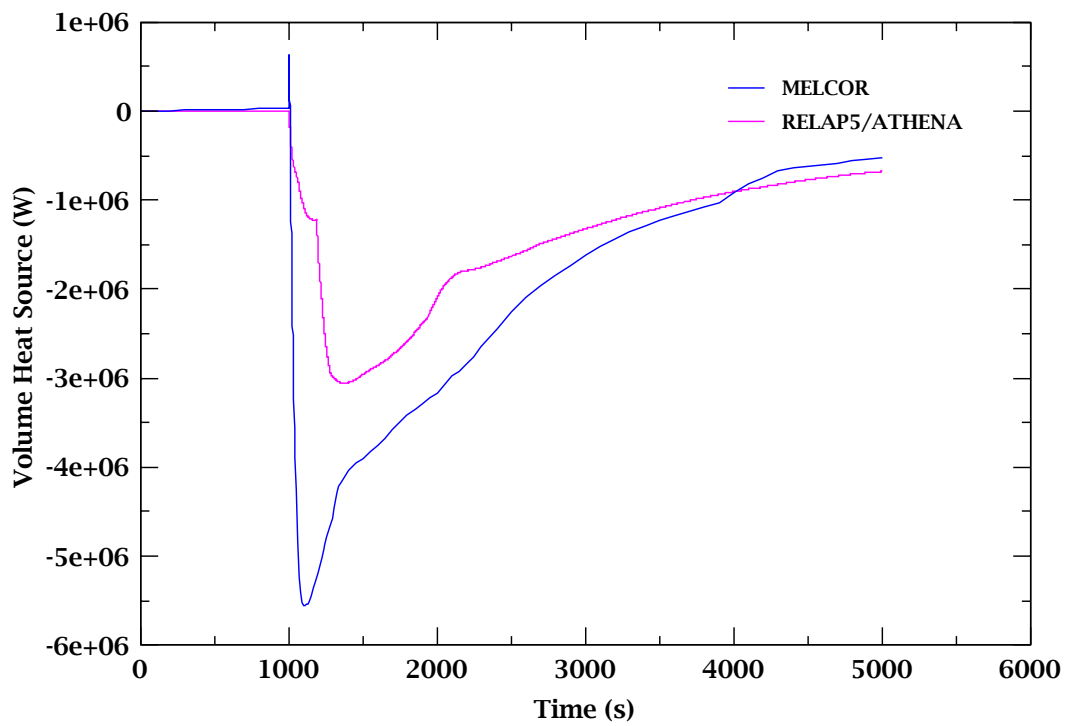
Figure 31. TCWS vault wall heat transfer rate to the atmosphere.

APPENDIX A

Listing of Dust Oxidation Functions

```
      REAL FUNCTION FUN2(PH2O,T,DELTA,RHODUST,DPMU, IERR)
C
      REAL*4 K1
      REAL*8 TRM
C
      DATA A, B, C, D, E, F, G, H /
     . 1.06036, 0.15610, 0.19300, 0.47635, 1.03587, 1.52996,
     . 1.76474, 3.89411 /
C  * * DENSITY IN KG/M3
      DATA RHODSTO / 1000. /
      DATA DPMUO / 2.1 /
      DATA PO / 1.0 /
      DATA TO / 293.0 /
      DATA EPSOK /108.9/
      DATA SIGAB / 2.809/
      DATA EPS  / 0.45 /
      DATA TAU2 / 0.64 /
      DATA RCON / 8.315 /
      DATA DELTAO / 2.78D-3 /
      DATA CAPPA /111.11 /
      DATA CH2OO / 27.7 /
C
      IF(DELTA  .LE.0.0) DELTA   = DELTAO
      IF(RHODUST.LE.0.0) RHODUST = RHODSTO
      IF(DPMU   .LE.0.0) DPMU    = DPMUO
C
      TSTAR   = TO/EPSOK
      OMEGAO  = A/TSTAR**B + C*EXP(-D*TSTAR) + E*EXP(-F*TSTAR)
     .                       + G*EXP(-H*TSTAR)
C
      CH2O  = PH2O/(RCON*T)
      P     = PH2O/1.E5
      TSTAR = T/EPSOK
      OMEGA = A/TSTAR**B + C*EXP(-D*TSTAR) + E*EXP(-F*TSTAR)
     .                       + G*EXP(-H*TSTAR)
C
      DAB  = 8.5D-5*(PO/P)*(T/TO)**1.5*(OMEGAO/OMEGA)
      DEFF = DAB*TAU2*EPS
C * * SPECIFIC AREA M2/KG
      ABET = 1000.*(1.6937 - 0.0336*DPMU)
      AOV  = ABET*RHODUST
C
      ROX = 0.1205D0*EXP(-13465.0/T)
      IF(T.GT.793.) THEN
      IF(T.LT.1140.) THEN
      ROX = 2.571D07*EXP(-28789.0/T)
                    ELSE
      ROX = 35.357D0*EXP(-13387.0/T)
                    ENDIF
                ENDIF
C
C * * * PRESSURE DEPENDENCE
      PRATIO = PH2O/0.86E5
      PMH2O = MIN(2.14,PRATIO**0.9)
      IF(PRATIO.GT.2.0) THEN
      PRATIO2 = PH2O/2.E5
      PMH2O = PMH2O*MIN(1.52,PRATIO2**0.6)
                ENDIF
      IF(PRATIO.GT.4.0) THEN
      PRATIO3 = PH2O/4.E5
      PMH2O = PMH2O*MIN(1.18,PRATIO3**0.4)
                ENDIF
```

```
      ROX = PMH2O*ROX
C
      K1 = ROX*AOV*CAPPA/CH2O0
C
      BCOEF = SQRT(K1/DEFF)
C
      TRM   = BCOEF*DELTA
C
      IF(DELTA .LT. DELTAO) THEN
      XL = DELTAO - DELTA
      CH2O = CH2O/(1. + XL*BCOEF*DTANH(TRM))
                          ENDIF
C
c      RH2O  =(K1*CH2O/BCOEF)*(DSINH(TRM) + DTANH(TRM)*(1.D0-DCOSH(TRM)))
      RH2O  =(K1*CH2O/BCOEF)* DTANH(TRM)
     .        +(K1*CH2O/BCOEF)*(DSINH(TRM) - DTANH(TRM)*DCOSH(TRM))
C
      RBE   = RH2O/CAPPA
C
      FUN2  = RBE
C
      RETURN
      END
      REAL FUNCTION FUN3(ROX,PH2O,T,ASURF,DT,IERR)
      REAL MBE, MH2, MH2O, MBEO
C
      DATA RHOBE / 1850.   /
      DATA MBE   / 9.0122  /
      DATA MH2   / 2.0141  /
      DATA MH2O  / 18.0135 /
      DATA MBEO  / 25.0116 /
      DATA RCON  / 1.98    /
C
      OXMH2  = 0.
      OXMH2O = 0.
      OXMCO  = 0.
      QOX    = 0.
C
C --- Beryllium/steam oxidation
C     Be + H2O --> BeO + H2
C
C * * Get hydrogen production and reaction energy
C
C
C * * * Beryllium
C
C        HFBEO in J/(kg-BeO)    ;  HFH20 in J/(kg-H2O)
C        ROX  in (kg-Be)/(m2*s) ;  QOX   in W/m2
C
C
      TOX = T
      TOX = MIN(2000.0, TOX )
      HFBEO = (-144220.+1.91*TOX/2.303
     .             +.00046*TOX**2+2.*1.24e5/TOX)*(4187./MBEO)
      HFH2O = (-56930.0-6.75*TOX/2.303
     .             +.00064*TOX**2-2.*0.08e5/TOX)*(4187./MH2O)
C
      OXMH2O= -DT*ROX*(MH2O/MBE)*HSMULT*ASURF
c      DELTHK = MAX(0.0, DT*ROX/RHOBE)
c      OXMH2O= -DT*ROX*(MH2O/MBE)*ASURF
      OXMH2 =  DT*ROX*(MH2/MBE)*ASURF
      QOX   = -(HFBEO-HFH2O*(MH2O/MBEO))*ROX*(MBEO/MBE)*ASURF
C
```

47

```
FUN3 = QOX
RETURN
END
```

APPENDIX B

Test Case MELCOR Input Deck Listing

```
      ***************************************************************************
      *    FEAT deasign according to DDDs 2001
      *    ITER-FEAT in-vessel LOCA:  Multiple in-vessel FW coolant leak
      *
      *eor* melgen
      ***************************************************************************
      *
      title  'ITER-FEAT multiple in-vessel LOCA'
      crtout
      outputfile   bedust.out
      diagfile     bedust.dia
      restartfile  bedust.res
      ***************************************************************************
      dttime  0.01
      ncg001  h2 4
      ncg002  o2 5
      ncg003  n2 6
      ncg004  co 7
      ncg005  co2 8
      ncg006  He  9            *for He leak from cryopums
      ***************************************************************************
      sc00001  4200    0.98        1   * Below Psat/Ptot use Standard MELCOR
      sc00003  4084     2000.      1   * laminar RE
      sc00004  4084    10000.      2   * turbulent Re
      ***************************************************************************
      ***************************************************************************
      ***************************************************************************
      *      Control Volumes for Plasma Chamber and Suppression System
      ***************************************************************************
      ***************************************************************************
      * * *  main plasma chamber volume CV100
      * * *  mlfr.9 = helium
      ***************************************************************************
      cv10000   plaschm  1   2   4
      cv10001   0        -2
      cv10002   0.0      0.0
      cv100a0   3
      cv100a1   pvol cf.400    zpol cf.406  tpol  cf.401
      cv100a2   tatm cf.401  ph2o cf.402  mlfr.6  cf.403
      *
      ***      altitude   volume
      *
      cv100b1   -4.15       0.0
      cv100b2   -3.65      80.0
      cv100b3    5.15     1150.0  * Total Vol. minus Jet Impingement Vol.
      *
      cf39000  ph20   tab-fun  1  1.0
      cf39001  0.
      cf39003  120
      cf39010  1.0  0.0    time
      *
      cf39500  temp   add   2   1.0
      cf39501  373.
      cf39510  0.05  0.0    hs-temp.0001101
      cf39511  0.95  0.0    cfvalu.395
      *
      cf40000  press   add  2  1.0
      cf40001  1.1e5
      cf40010  0.0 700.    time
      cf40011  1.0  0.0    cfvalu.390
      *
      cf40100  temp   add   2   1.0
      cf40101  373.
```

```
cf40110  0.5  0.0    hs-temp.0001101
cf40111  0.5  0.0    hs-temp.0000101
*
cf40200  ph20   equals  1  1.0
cf40201  0.
cf40210  1.0  0.0    cfvalu.390
*
cf40300  mfn2   equals  1   1.0
cf40301  1.0
cf40310  0.0  1.0    time
*
cf40600  mfh2o   equals  1   1.0
cf40601  -4.15
cf40610  0.0  -4.15   time
*
tf12000  FWRadQ  4  1.0
tf12010    0.0   0.0       *
tf12013  1000.0   0.0      *
tf12015  1001.0   1.0e5    *
tf12016  1001.1   1.0e5
*
********************************************************************************
*          Inboard first wall CV005
********************************************************************************
cv00500   fwin  1  2  1
cv00501   0    -1
cv00502   0.0   3.235
cv00503   0.3114
cv005a0   2
cv005a1   pvol 1.8466e6  ph2o  1.8466e6  tatm  406.959  tpol  406.959
cv005a2   mfrc.1 1.0    mfrc.2 0.0    mfrc.3  0.0
*
***       altitude   volume
*
cv005b1   -2.7         0.0
cv005b2    5.0         2.3976
********************************************************************************
*-------------------------------------------------------------------------------
*          FW/BLK HEAT STRUCTURES for 1 loop (damaged)
*-------------------------------------------------------------------------------
********************************************************************************
********************************************************************************
*          Inboard first wall (be+cu)1 loop  hs00001
********************************************************************************
hs00001000       5     1     -1
hs00001001     fwbe
hs00001002     -2.7      1.0
hs00001100     -1       1      0.0
hs00001101     0.005   2
hs00001102     0.010   3
hs00001103     0.01472  4
hs00001104     0.01963  5
hs00001200     -1
hs00001201      beryllium  2
hs00001202      copper     4
hs00001300     201    -1    0.2703
hs00001301     1.0     4
hs00001400    7014  100       ext   0.0    1.0
hs00001401     0.6    gray-gas-a  5.0
hs00001500     221.4    7.70      7.70
hs00001600    1   5       int   0.0    1.0
hs00001601     0.2    gray-gas-a  0.01
hs00001700     221.4    0.01       7.7
```

51

```
hs00001800        -1
hs00001801     440.13      1
hs00001802     432.84      2
hs00001803     424.86      3
hs00001804     421.04      4
hs00001805     416.72      5
****************************************************************************
hs00011000        6     1     -1
hs00011001     fwbedust
hs00011002     -2.7      1.0
hs00011100     -1       1      0.0
hs00011101     0.002    2
hs00011102     0.007    3
hs00011103     0.012    4
hs00011104     0.01672  5
hs00011105     0.02163  6
hs00011200       -1
hs00011201      bedust   1
hs00011202      beryllium  3
hs00011203      copper     5
hs00011300      201     -1    0.2703
hs00011301      0.0      1
hs00011302      1.0      5
hs00011400     7706  100       ext    0.0    1.0
hs00011401     0.6    gray-gas-a  5.0
hs00011500     221.4    7.70      7.70
hs00011600     1    5       int    0.0    1.0
hs00011601     0.2    gray-gas-a  0.01
hs00011700     221.4   0.01      7.7
hs00011800       -1
hs00011801     450.13      1
hs00011802     440.13      2
hs00011803     432.84      3
hs00011804     424.86      4
hs00011805     421.04      6
hs00011806     416.72      6
*
cf70400  roxbe     fun2   5  1.0    * radiation+conduction function
cf70401  0.0                         * initial value
cf70410  1.0  0.0     cvh-p.100      * pressure
cf70411  1.0  0.0     cfvalu.395     * temp
*cf70411  1.0  0.0     hs-temp.0001101   * temp
cf70412  0.0  0.0     time           *
cf70413  0.0  0.0     time           *
cf70414  0.0  0.0     time           *
*
cf70500  roxbe     fun3   5  1.0    * radiation+conduction function
cf70501  0.0                         * initial value
cf70510  1.0  0.0     cfvalu.704     * rox
cf70511  1.0  0.0     cvh-p.100      * pressure
cf70512  1.0  0.0     cfvalu.395  * temp
*cf70512  1.0  0.0     hs-temp.0001101   * temp
cf70513  0.0 221.4    time           * area
cf70514  0.0  0.0     time           *
****************************************************************************
cf70600  FWSurfQ   add  2  1.0
cf70601  44.28e6
cf70610  1.0  0.0  cfvalu.13   * Radiant Heat Load
cf70611  1.0  0.0  cfvalu.705  * oxidation
*
****************************************************************************
cf01300  FWRadQ  tab-fun  1  1.0
cf01301  44.28e6                        * initial value
```

```
cf01303  130                              * table 130
cf01310  1.0  0.0  time
*************************************************************************
cf01400  FWSurfQ  add  2  1.0
cf01401  44.28e6
cf01410  1.0  0.0  cfvalu.13   * Radiant Heat Load
cf01411  0.0  0.0  time        * No Credit for Jet Impingement Cooling
*************************************************************************
tf13000  FWRadQ  7  1.0
tf13010    0.0   44.28e6  * (0.20 MW/m2)(221.4 m2) = 44.28 MW
tf13011   989.9  44.28e6  *
tf13012   990.0  46.708e6  * 10% Power Increase
tf13013  1000.0  46.708e6   *
tf13014  1000.1  130.23e6  * Plasma Disruption
tf13015  1001.0  130.23e6  * (0.129 GJ)/(1 s)x1.0 =130.23 MW
tf13016  1001.1   0.0e6
*************************************************************************
*
*   **** NUCLEAR HEATING TABLES FOR FW/BLK REGION
*
*************************************************************************
*************************************************************************
*****    hs00001
*************************************************************************
tf20100      hs1    17        1.00   0.0
tf20110     0.0     75.635e6
tf20111   989.99    75.635e6
tf20112   990.00    83.823e6
tf20113  1000.0     83.823e6
tf20114   1001.    3.0485e6
tf20115   1300.    1.9946e6
tf20116   2800.    0.6258e6
tf20117   4600.    0.4159e6
tf20118  11800.    0.3495e6
tf20119  19000.    0.3137e6
tf20120  37000.    0.2427e6
tf20121  87400.    0.1236e6
tf20122   2.6e5    0.0279e6
tf20123   6.6e5    0.0203e6
tf20124  2.631e6   0.0200e6
tf20125  7.881e6   0.0196e6
tf20136  3.15e7    0.0177e6
*************************************************************************
*
*********************************************************
*
mpmat00300        beryllium *SADL 3-96
mpmat00301        rho       8
mpmat00302        cps       9
mpmat00303        thc       10
*
tf00800  rho  2        1.0     0.0
tf00801  0     0
tf008a3  300.0 1821.117
tf008b6  1500.0 1821.117
*
tf00900  cps  14       1.0     0.0
tf00901  0     0
tf009a2 290.0 1807.281
tf009a3 300.0 1829.622
tf009a4 400.0 2117.856
tf009a5 500.0 2353.554
tf009a6 600.0 2544.364
```

```
tf009a7 700.0 2697.936
tf009a8 800.0 2821.918
tf009a9 900.0 2923.960
tf009b1 1000.0 3011.709
tf009b2 1100.0 3092.816
tf009b3 1200.0 3174.928
tf009b4 1300.0 3265.694
tf009b5 1400.0 3372.763
tf009b6 1500.0 3465.614
*
tf01000  thc   14     1.0      0.0
tf01001  0     0
tf010a2  290.0 184.513
tf010a3  300.0 182.709
tf010a4  400.0 159.481
tf010a5  500.0 140.569
tf010a6  600.0 125.367
tf010a7  700.0 113.268
tf010a8  800.0 103.666
tf010a9  900.0 95.955
tf010b1  1000.0 89.529
tf010b2  1100.0 83.781
tf010b3  1200.0 78.105
tf010b4  1300.0 71.896
tf010b5  1400.0 64.546
tf010b6  1500.0 58.112
*
mpmat00400        copper   *SADL 3-96
mpmat00401        rho      11
mpmat00402        cps      12
mpmat00403        thc      13
*
tf01100  rho   2      1.0      0.0
tf01101  0     0
tf011a3  300.0 8858.071
tf011a8  800.0 8858.071
*
tf01200  cps   7      1.0      0.0
tf01201  0     0
tf012a2 290.0 384.193
tf012a3 300.0 385.249
tf012a4 400.0 399.164
tf012a5 500.0 410.892
tf012a6 600.0 420.431
tf012a7 700.0 427.782
tf012a8 800.0 431.767
*
tf01300  thc   12     1.0      0.0
tf01301  0     0
tf013a2  290.0 348.620
tf013a3  300.0 347.751
tf013a4  400.0 335.303
tf013a5  500.0 322.780
tf013a6  600.0 310.181
tf013a7  700.0 297.506
tf013a8  800.0 284.756
tf013a9  900.0 271.931
tf013b1  1000.0 259.030
tf013b2  1100.0 246.053
tf013b3  1200.0 233.001
tf013b4  1300.0 223.426
*
*
```

```
mpmat01700    bedust
mpmat01701    rho  208
mpmat01702    cps  209
mpmat01703    thc  210
*
*
tf20800   rho   2          0.55     0.0
tf20801   0      0
tf208a3  300.0  1821.117
tf208b6  1500.0 1821.117
*
tf20900   cps   14         1.0      0.0
tf20901   0      0
tf209a2 290.0 1807.281
tf209a3 300.0 1829.622
tf209a4 400.0 2117.856
tf209a5 500.0 2353.554
tf209a6 600.0 2544.364
tf209a7 700.0 2697.936
tf209a8 800.0 2821.918
tf209a9 900.0 2923.960
tf209b1 1000.0 3011.709
tf209b2 1100.0 3092.816
tf209b3 1200.0 3174.928
tf209b4 1300.0 3265.694
tf209b5 1400.0 3372.763
tf209b6 1500.0 3465.614
*
tf21000   thc   25    1.0        0.0
tf21001   0      0
tf210a2  3.7300E+02  2.6828E-01
tf210a3  4.2300E+02  3.0210E-01
tf210a4  4.7300E+02  3.4032E-01
tf210a5  5.2300E+02  3.8064E-01
tf210a6  5.7300E+02  4.2250E-01
tf210a7  6.2300E+02  4.6551E-01
tf210a8  6.7300E+02  5.0937E-01
tf210a9  7.2300E+02  5.5380E-01
tf210b1  7.7300E+02  5.9858E-01
tf210b2  8.2300E+02  6.4346E-01
tf210b3  8.7300E+02  6.8824E-01
tf210b4  9.2300E+02  7.3269E-01
tf210b5  9.7300E+02  7.7659E-01
tf210b6  1.0230E+03  8.1969E-01
tf210b7  1.0730E+03  8.6173E-01
tf210b8  1.1230E+03  9.0240E-01
tf210b9  1.1730E+03  9.4138E-01
tf210c1  1.2230E+03  9.7827E-01
tf210c2  1.2730E+03  1.0127E+00
tf210c3  1.3230E+03  1.0440E+00
tf210c4  1.3730E+03  1.0718E+00
tf210c5  1.4230E+03  1.0952E+00
tf210c6  1.4730E+03  1.1134E+00
tf210c7  1.5230E+03  1.1252E+00
tf210c8  1.5600E+03  1.1289E+00
.
************************************************
*eor* melcor
*
title  'ITER-FEAT multiple in-vessel LOCA'
crtout
* dtsummary
outputfile   bedust.out
```

```
diagfile     bedust.dia
restartfile  bedust.res
messagefile  bedust.mes
plotfile     bedust.ptf
*
jobid  'ITER-FEAT multiple in-vessel LOCA'
nocopy
cymesf        20 100
cpuleft       20.0
cpulim        1.e10
tend      1050.
*tend         1.000e6
warninglevel  1,2,1
*forceplot    1.0e-6,0
*restart      10083
*cvhtrace
*
*          TIME    DTMAX    DTMIN    DTEDT    DTPLT    DTRST
time1       0.0     0.01    1.e-8    100.0    5.0    2000.0
time2     100.0     0.1     1.e-8    100.0    5.0    2000.0
time3    1000.0     0.01    1.e-8    100.0    5.0    2000.0
*
.
*
```

APPENDIX C

Changes Made to MELCOR Wet Bypass input Deck

```
*
*  Be dust oxidation control functions
*
*
cf58500  mratio   divide 2  2.78e-3  0.0     *
cf58501  2.78e-3                 *Initial value
cf58510  0.0       100.0    time         *
cf58511  1.0         0.0   cfvalu.603        * mo/m
*
cf58600  fwevap      L-GT 2 1.0  0.0        *
cf58601  .false.            *Initial value
cf58605  latch              * first opening only
cf58606  2  'Be Dust Evap   '       * message
cf58610  1.0 0.0    hs-temp.0190201      * Be bulk temperature
cf58611  0.0 1.560e3     time        * Be Dust surface melt 1560 C
*
cf58700  BoT   power-r 1  1.0  0.0  *
cf58701  20.0                    *Initial value
cf58703  0.5                     *
cf58710  1.0      0.0    hs-temp.0190201   *  T^1/2
*
cf58800  BoT   multiply 2  1.0  0.0  *
cf58801  0.0                    *Initial value
cf58810  1.0      0.0    hs-temp.0190201   *  T
cf58811  0.0   0.00575 time         *  B
*
cf58900  pbe        EXP 1 1.31e-2 0.0   * A x exp(BxT)
cf58901  0.                 * initial
cf58910  1.0 0.0    cfvalu.588        *
*
cf59000  SWTCHPon  l-a-ifte  3  1.0
cf59001  1.0
cf59010  1.0  0.0  cfvalu.586
cf59011  1.0  0.0  cfvalu.589
cf59012  0.0  0.0  time
*
cf59100  Qevap   divide 2  1.3e9  0.0      *  area *hfg
cf59101  0.0                    *Initial value
cf59110  1.0         0.0   cfvalu.587      *  1/T^1/2
cf59111  1.31e-2    0.0   cfvalu.590       *  A x P
*
cf59200  crate    min 2 1.0 0.0  *limit temperature to melt
cf59201  400.                 * initial mass
cf59210  1.0 0.0    hs-temp.0190201  *
cf59211  0.0 1560. time
*
cf59300  BoT   divide 2  1.0  0.0  * -B/T
cf59301  0.0                    *Initial value
cf59310  1.0      0.0    hs-temp.0190201   *  1/T
*cf59310  1.0      0.0  cfvalu.592     *  1/T
cf59311  0.0 -13387.  time         *  -B
*
cf59400  SurRox    EXP 1 35.36 0.0    * A x exp(-B/T)
cf59401  100.                 * initial mass
cf59410  1.0 0.0    cfvalu.593        *
*
cf59500  oldmass    EQUALS 1 1.0 0.0  *FW Surface Temperature
```

58

```
cf59501  100.                            * initial mass
cf59510  1.0 0.0    cfvalu.603           *
*
cf59600  stmlim   divide 2 2.7778e-2  0.0 * steam limit/As
cf59601  0.0                          *Initial value
cf59610  1.0      0.0    dt           *  dt
cf59611  1.0      0.0    cvh-mass.3.100    *  MeH2O
*
cf59700  belim    divide 2 2.7778e-2  0.0 * be limit/As
cf59701  0.0                          *Initial value
cf59710  1.0      0.0    dt           *  dt
cf59711  1.0      0.0    cfvalu.595   *  Mebe
*
cf59800  fwoutb       L-GT 2 1.0  0.0        *
cf59801  .false.               *Initial value
cf59805  latch                 * first opening only
cf59806  2  'Be Dust T>1570 C'        * message
cf59810  1.0 0.0    hs-temp.0190202       * Be bulk temperature
cf59811  0.0 1.570e3    time          * Be Dust surface melt 1570 C
*
cf59900  roxbe     fun2   5  1.0     * be oxidation function 1
cf59901  0.0                          * initial value
cf59910  1.0  1.0    cvh-ppart.3.100     * pressure
cf59911  1.0  0.0    hs-temp.0190201     * temp
*cf59911  1.0  0.0    cfvalu.592     * temp
cf59912  1.0  0.0    cfvalu.585     * dx
*cf59912  0.0  2.78e-3 time          * dx
cf59913  0.0 1000.    time           * rhodust
cf59914  0.0  2.1     time           * dp (microns)
*
cf60000  WhichRox  l-a-ifte  3  1.0
cf60001  1.0
cf60010  1.0  0.0  cfvalu.598
cf60011  1.0  0.0  cfvalu.594
cf60012  1.0  0.0  cfvalu.599
*
cf60100  crate    min 3 1.0 0.0  *controlling rate
cf60101  0.                 * initial mass
cf60110  1.0 0.0    cfvalu.600         *
cf60111  1.0 0.0    cfvalu.596
cf60112  1.0 0.0    cfvalu.597
*
cf60200  beloss   multiply 3  1.0   0.0 *
cf60201  0.0                          *Initial value
cf60210  1.0      0.0    cfvalu.601   *  rbeox
cf60211  0.0   36.0    time           *  area
cf60212  1.0      0.0    dt           *  dt
*
cf60300  oldmass    add 2 1.0 0.0  *FW Surface Temperature
cf60301  100.                        * initial mass
cf60310  1.0 0.0    cfvalu.595         * mobe
cf60311 -1.0 0.0    cfvalu.602         * dmbe
*
cf60500  qoxbe     fun3   5  1.0     * be oxidation function 2
cf60501  0.0                          * initial value
cf60510  1.0  0.0    cfvalu.601     * rox
cf60511  1.0  0.0    cvh-ppart.3.100     * pressure h2o
```

```
cf60512  1.0  0.0     hs-temp.0190201 * temp
*cf60512  1.0  0.0      cfvalu.592     * temp
cf60513  0.0 36.0     time          * area
cf60514  0.0  0.0     time          * not used
*
cf60600  Qrad          FUN1  5 1.0 0.0   *conduction
cf60601  0.0                              *initial value
cf60610  1.0       0.0    hs-temp.0190201    *temp1
cf60611  0.0    420.0      TIME     *temp2
cf60612  0.0       0.0     TIME          *solid%*conductivity/deltax
cf60613  0.0       0.3     TIME          *emissivity*(1-solid%)
cf60614  0.0      36.0     TIME          *area
*
cf60700  NetQ       add 3 1.0 0.0  *FW Surface Temperature
cf60701  100.                       * initial mass
cf60710  1.0 0.0    cfvalu.605        * Qox
cf60711 -1.0 0.0    cfvalu.606        * Qrad
cf60712 -1.0 0.0    cfvalu.591        * Qevap
*
cf61000  h2prod  multiply 4 1.0  0.0 *
cf61001  0.0                          *Initial value
cf61010  1.0       0.0    cfvalu.601    * rbeox
cf61011  0.0 2.0141     time          * MeH2
cf61012  0.0  0.11096  time          * 1./MwBe = 1./9.0122
cf61013  0.0   36.0     time          * area
*
cf61100  fetemp    EQUALS 1 1.0 0.0  *FW Surface Temperature
cf61110  1.0 0.0    hs-temp.0090101  *
*
cf61200  h2osink  multiply 4 -1.0  0.0 *
cf61201  0.0                          *Initial value
cf61210  1.0       0.0    cfvalu.601    * rbeox
cf61211  0.0 18.0135    time          * MeH2
cf61212  0.0  0.11096  time          * 1./MwBe = 1./9.0122
cf61213  0.0   36.0     time          * area
*
cf61300  tvtemp     EQUALS 1 1.0 0.0   *Vapor Temperature
cf61310  1.0 0.0    cvh-tvap.100        *
*
*              first wall (be dust+cu)  hs01901 (outside)
*************************************************************************
*******
hs01901000    5    1     -1
hs01901001  fwbedusto
hs01901002  -3.25   1.0
hs01901100  -1      1     0.0
hs01901101  0.00278  3
hs01901102  0.01241  5
hs01901200   -1
hs01901201  bedust      1
hs01901202  bedustIF    2
hs01901203  copper      4
hs01901300  9629  -1    1.0
hs01901301   0.0   1
hs01901302   1.0   2
hs01901303   0.0   4
hs01901400  7830 100     ext    0.0    1.0
```

```
*hs01901401  0.6   gray-gas-a  5.0
hs01901500  18.0    8.25      8.25
hs01901600  7635   901     int    0.0    1.0
hs01901601  0.2   gray-gas-a  0.01
hs01901700  18.0   0.01     8.25
hs01901800   -1
hs01901801  437.32      1
hs01901802  429.68      2
hs01901803  421.24      3
hs01901804  417.15      4
hs01901805  412.48      5
*************************************************************************
*******
*                 first wall (be dust+cu)  hs01902 (inside)
*************************************************************************
*******
hs01902000    5   1     -1
hs01902001  fwbedusti
hs01902002  -3.25   1.0
hs01902100  -1     1    0.0
hs01902101  0.00278  3
hs01902102  0.01241  5
hs01902200   -1
hs01902201   bedust      1
hs01902202   bedustIF    2
hs01902203   copper      4
hs01902300  9619   -1    1.0
hs01902301   0.0   1
hs01902302   1.0   2
hs01902303   0.0   4
hs01902400  7820  100      ext    0.0    1.0
*hs01902401  0.6   gray-gas-a  5.0
hs01902500  18.0    8.25      8.25
hs01902600  7636   901     int    0.0    1.0
hs01902601  0.2   gray-gas-a  0.01
hs01902700  18.0   0.01     8.25
hs01902800   -1
hs01902801  437.32      1
hs01902802  429.68      2
hs01902803  421.24      3
hs01902804  417.15      4
hs01902805  412.48      5
*************************************************************************
*******
hs00901300  9639   -1    1.0
hs00901301   0.0   1
hs00901302   1.0   2
hs00901303   0.0   4
----
hs00901500     644.0      8.25      8.25
---
hs00901700     644.0      0.01     8.25
---
cf91200  seg1b        FUN1  5 0.947 0.0    *radiation+conduction
function
---
*
```

```
cf63500  seg1b         FUN1  5 0.0265 0.0    *radiation+conduction
function
cf63501  0.0                           *initial value
cf63510  1.0 0.0       hs-temp.0090401       *temp1
cf63511  1.0 0.0       hs-temp.0190105       *temp2
cf63512  0.0  7.696e4  TIME               *solid%*conductivity/deltax
cf63513  0.0  0.093    TIME               *emissivity*(1-solid%)
cf63514  1.0 0.0       cfvalu.900      *area
*
cf63600  seg1b         FUN1  5 0.0265 0.0    *radiation+conduction
function
cf63601  0.0                           *initial value
cf63610  1.0 0.0       hs-temp.0090401       *temp1
cf63611  1.0 0.0       hs-temp.0190205       *temp2
cf63612  0.0  7.696e4  TIME               *solid%*conductivity/deltax
cf63613  0.0  0.093    TIME               *emissivity*(1-solid%)
cf63614  1.0 0.0       cfvalu.900      *area
3770c3541
---
cf91600  seg4f         add  3  1.0
---
cf91611 -1.0 0.0       cfvalu.635
cf91612 -1.0 0.0       cfvalu.636
---
cf92000  FWSurfQ  add  3  1.0
cf92001  129.40e6
cf92010  0.947  0.0  cfvalu.913   * Radiant Heat Load
---
cf92012  1.0  0.0  cfvalu.825  * Qcond
---
*************************************************************************
*******
*              dust to dust
*************************************************************************
*******
cf61500  Tave  add  2  1.0
cf61501  0.0
cf61510  0.5       0.0  hs-temp.0190202    * T1
cf61511  0.5       0.0  hs-temp.0190102    * T2
*
***** k ave
*
cf61600  kave1    tab-fun  1  1333.33       * 1/dx
cf61601  0.55                          * initial value
cf61603  026                           * table 26
cf61610  1.0  0.0  cfvalu.615          * Tave
*
**** Q conduction
*
cf61700  Qcondi       FUN1  5 1.0 0.0   *conduction
cf61701  0.0                           *initial value
cf61710  1.0       0.0    hs-temp.0190202    *temp1
cf61711  1.0       0.0    hs-temp.0190102    *temp2
cf61712  1.0       0.0    cfvalu.616
*solid%*conductivity/deltax
cf61713  0.0       0.0    TIME            *emissivity*(1-solid%)
cf61714  0.0       86.7   TIME            *area
```

```
*
***** nuc heating
*
cf61800  NucHeat  tab-fun  1  1.0
cf61801  0.0                              * initial value
cf61803  201                              * table 201
cf61810  1.0  0.0  time            *
*
***** net heating
*
cf61900  Qneti  add  2  1.0
cf61901  0.0
*cf61910  0.0265 0.0  cfvalu.618    * Qnuc
cf61910  0.0      0.0  cfvalu.618       * Qnuc
cf61911 -1.0      0.0  cfvalu.617       * Qc
*
* * * surface
*
cf81500  Tave  add  2  1.0
cf81501  0.0
cf81510  0.5       0.0  hs-temp.0190201  * T1
cf81511  0.5       0.0  hs-temp.0190101  * T2
*
***** k ave
*
cf81600  kave1    tab-fun  1  1333.33       * 1/dx
cf81601  0.55                             * initial value
cf81603  026                              * table 26
cf81610  1.0  0.0  cfvalu.815         * Tave
*
**** Q conduction
*
cf81700  Qcondi       FUN1   5 1.0 0.0   *conduction
cf81701  0.0                              *initial value
cf81710  1.0       0.0    hs-temp.0190201    *temp1
cf81711  1.0       0.0    hs-temp.0190101    *temp2
cf81712  1.0       0.0    cfvalu.816
*solid%*conductivity/deltax
cf81713  0.0       0.0    TIME             *emissivity*(1-solid%)
cf81714  0.0       43.3   TIME             *area
*
cf82000  FWSurfQ  add  3  1.0
cf82001  3.604e6
cf82010  0.0265 0.0  cfvalu.913  * Radiant Heat Load
cf82011  0.5      0.0  cfvalu.607  * bedust oxidation
*cf82011  0.5      0.0  cfvalu.605  * bedust oxidation
cf82012 -1.0      0.0  cfvalu.817  * conduction
************************************************************************
*******
*             dust to tile
************************************************************************
*******
cf51800  sigma  equals  1  1.0
cf51801  0.0
cf51810  0.0      2.8e-6    time        * sigma
*
cf51900  pg   max 2  1.0
```

63

```
cf51901  0.0
cf51910  0.0   10.0   time             * pmin
cf51911  1.0       0.0  cvh-ppart.3.100   * pg
*
cf52000  pgsigma  multiply  2  1.0
cf52001  0.0
cf52010  1.0       0.0  cfvalu.518        * sigma
cf52011  1.0       0.0  cfvalu.519        * pg
*
cf52100  Tave  add  2  1.0
cf52101  0.0
cf52110  0.5       0.0  hs-temp.0190102   * T1
cf52111  0.5       0.0  hs-temp.0090102   * T2
*
***** k ave
*
cf52200  Kave2   tab-fun  1  37.435    * 1/dx + hg
cf52201  150.                          * initial value
cf52203  010                           * table 10
cf52210  1.0  0.0  cfvalu.521          * Tave
*
cf52300  Bcoef  tab-fun  1  1.0
cf52301  0.03
cf52303  5
cf52310  1.0       0.0  cfvalu.521         * B at Tave
*
tf00500  Bc   11     1.0       0.0
tf00501  0     0
tf005a2  380.0  2.25E-02
tf005a3  400.0  2.45E-02
tf005a4  450.0  2.98E-02
tf005a5  500.0  3.49E-02
tf005a6  550.0  4.06E-02
tf005a7  600.0  4.69E-02
tf005a8  650.0  5.29E-02
tf005a9  700.0  5.93E-02
tf005b1  750.0  6.57E-02
tf005b2  800.0  7.29E-02
tf005b3  850.0  8.00E-02
*
cf52400  kg   tab-fun  1  1.0
cf52401  0.02
cf52403  2
cf52410  1.0       0.0  cfvalu.521     * kgas at Tave
*
tf00200  kg   11     1.0       0.0
tf00201  0     0
tf002a2  380.0  0.0246
tf002a3  400.0  0.0261
tf002a4  450.0  0.0299
tf002a5  500.0  0.0339
tf002a6  550.0  0.0379
tf002a7  600.0  0.0422
tf002a8  650.0  0.0464
tf002a9  700.0  0.0505
tf002b1  750.0  0.0549
tf002b2  800.0  0.0592
```

```
tf002b3  850.0  0.0637
*
cf52500  denom  divide 2  1.0 1.0  * add 1
cf52501  0.0
cf52510  1.0      0.0  cfvalu.520        * p*sigma
cf52511  1.0      0.0  cfvalu.523        * Bc
*
cf52600  hg    divide 2  1.0  0.0   * eps*sigma
cf52601  0.0
cf52610  2.7      0.0    cfvalu.518 * 2.7 sigma
cf52611  1.0      0.0    cfvalu.524 * kg
*
*cf52700  hgape  divide 2  1.0
*cf52701  0.0
*cf52710  1.0  0.0  cfvalu.525        * denom
*cf52711  1.0  0.0  cfvalu.526         * hgap
*
cf52700  hgap  equals 1  1.0
cf52701  0.0
cf52710  0.0  250.0  time          * hgap
*
cf52800  esps  equals 1  1.0
cf52801  0.0
cf52810  0.0  0.135  time          * eps=0.3*.45
*
cf62200  hsum  add  2  1.0
cf62201  0.0
cf62210  1.0      0.0  cfvalu.522        * h1
cf62211  1.0      0.0  cfvalu.527        * h2
*
cf62300  hsum    multiply  2  1.0  0.0       *
cf62301  0.0
cf62310  1.0      0.0   cfvalu.522     *
cf62311  1.0      0.0   cfvalu.527     * h1*h2
*
cf62400  valvfr1   DIVIDE  2  1.0  0.0       *
cf62401  0.0
cf62410  1.0      0.0   cfvalu.622     * h1+h2
cf62411  1.0      0.0   cfvalu.623     * h1*h2
*
cf62500  Qcondo       FUN1  5 1.0 0.0   *Conduction
cf62501  0.0                            *initial value
cf62510  1.0      0.0   hs-temp.0190102    *temp1
cf62511  1.0      0.0   hs-temp.0090102    *temp2
cf62512  1.0      0.0   cfvalu.624     *solid%*conductivity/deltax
cf62513  1.0      0.0   cfvalu.528     *emissivity*(1-solid%) .3*.45
cf62514  0.0  86.7     TIME         *area
*
***** net heating
*
cf62900  Qneti  add  3  1.0
cf62901  0.0
*cf62910  0.0265 0.0  cfvalu.618    * Qnuc
cf62910  0.0      0.0  cfvalu.618       * Qnuc
cf62911  1.0      0.0  cfvalu.617       * Qci
cf62912 -1.0      0.0  cfvalu.625       * Qco
*
```

```
***************
*
cf79000  Tave  add  2  1.0
cf79001  0.0
cf79010  0.5      0.0  hs-temp.0190101   * T1
cf79011  0.5      0.0  hs-temp.0090101   * T2
*
***** k ave
*
cf79100  Kave2   tab-fun  1  37.435   * 1/dx + hgap
cf79101  150.                          * initial value
cf79103  010                           * table 10
cf79110  1.0  0.0  cfvalu.790          * Tave
*
cf82200  hsum  add  2  1.0
cf82201  0.0
cf82210  1.0      0.0  cfvalu.791        * h1
cf82211  1.0      0.0  cfvalu.527        * h2
*
cf82300  valvfr1   multiply  2  1.0  0.0      *
cf82301  0.0
cf82310  1.0      0.0  cfvalu.791      *
cf82311  1.0      0.0  cfvalu.527      * h1*h2
*
cf82400  valvfr1   DIVIDE  2  1.0  0.0      *
cf82401  0.0
cf82410  1.0      0.0  cfvalu.822     * h1+h2
cf82411  1.0      0.0  cfvalu.823     * h1*h2
*
cf82500  Qcondo        FUN1   5 1.0 0.0   *Conduction
cf82501  0.0                              *initial value
cf82510  1.0      0.0    hs-temp.0190101    *temp1
cf82511  1.0      0.0    hs-temp.0090101    *temp2
cf82512  1.0      0.0    cfvalu.824    *solid%*conductivity/deltax
cf82513  1.0      0.0    cfvalu.528    *emissivity*(1-solid%) .3*.45
cf82514  0.0   43.3      TIME          *area
*
cf83000  FWSurfQ  add  4  1.0
cf83001  3.604e6
cf83010  0.0265 0.0  cfvalu.913   * Radiant Heat Load
cf83011  0.5      0.0  cfvalu.607  * bedust oxidation
*cf83011  0.5      0.0  cfvalu.605  * bedust oxidation
cf83012 -1.0      0.0  cfvalu.825 * Qco
cf83013 1.0      0.0  cfvalu.817 * Qci
---
**************************************************************************
*******
*                tile
**************************************************************************
*******
*
***** net heating
*
cf63900  Qneti  add  2  1.0
cf63901  0.0
*cf63910  0.947  0.0  cfvalu.618    * Qnuc
cf63910  1.0      0.0  cfvalu.618        * Qnuc
```

```
cf63912  1.0       0.0   cfvalu.625        * Qci
---
cv100c3       mass.4     610    3   * dust oxidation sources
cv100c4       te         611    9
cv100c5       mass.3     612    3
cv100c6       te         613    9
---
***
*
mpmat01700    bedust
mpmat01701    rho  24
mpmat01702    cps  25
mpmat01703    thc  26
*
*
tf02400   rho  2  0.55   0.0
tf02401   0      0
tf024a3   300.0  1000.0
tf024b6   1500.0 1000.0
*
tf02500   cps  17      1.0      0.0
tf02501   0      0
tf025a2 290.0 1807.281
tf025a3 300.0 1829.622
tf025a4 400.0 2117.856
tf025a5 500.0 2353.554
tf025a6 600.0 2544.364
tf025a7 700.0 2697.936
tf025a8 800.0 2821.918
tf025a9 900.0 2923.960
tf025b1 1000.0 3011.709
tf025b2 1100.0 3092.816
tf025b3 1200.0 3174.928
tf025b4 1300.0 3265.694
tf025b5 1400.0 3372.763
tf025b6 1500.0 3465.614
tf025b7 1560.1 1.3e5          * heat of fusion over 10 C
tf025b8 1570.1 1.3e5
tf025b9 1570.2 3465.614
*
tf02600   thc  25      1.0      0.0
tf02601   0      0
tf026a2  3.7300E+02  2.6828E-01
tf026a3  4.2300E+02  3.0210E-01
tf026a4  4.7300E+02  3.4032E-01
tf026a5  5.2300E+02  3.8064E-01
tf026a6  5.7300E+02  4.2250E-01
tf026a7  6.2300E+02  4.6551E-01
tf026a8  6.7300E+02  5.0937E-01
tf026a9  7.2300E+02  5.5380E-01
tf026b1  7.7300E+02  5.9858E-01
tf026b2  8.2300E+02  6.4346E-01
tf026b3  8.7300E+02  6.8824E-01
tf026b4  9.2300E+02  7.3269E-01
tf026b5  9.7300E+02  7.7659E-01
tf026b6  1.0230E+03  8.1969E-01
tf026b7  1.0730E+03  8.6173E-01
```

```
tf026b8  1.1230E+03  9.0240E-01
tf026b9  1.1730E+03  9.4138E-01
tf026c1  1.2230E+03  9.7827E-01
tf026c2  1.2730E+03  1.0127E+00
tf026c3  1.3230E+03  1.0440E+00
tf026c4  1.3730E+03  1.0718E+00
tf026c5  1.4230E+03  1.0952E+00
tf026c6  1.4730E+03  1.1134E+00
tf026c7  1.5230E+03  1.1252E+00
tf026c8  1.5600E+03  1.1289E+00
*
mpmat01800    bedustIF
mpmat01801    rho  24
mpmat01802    cps  25
mpmat01803    thc  27
*
*
*tf02700  thc 25    1.0      0.0   * has hg=500 for interface
*tf02701  0    0
*tf027a2  3.7300E+02  1.936E-01
*tf027a3  4.2300E+02  2.106E-01
*tf027a4  4.7300E+02  2.285E-01
*tf027a5  5.2300E+02  2.459E-01
*tf027a6  5.7300E+02  2.628E-01
*tf027a7  6.2300E+02  2.788E-01
*tf027a8  6.7300E+02  2.939E-01
*tf027a9  7.2300E+02  3.082E-01
*tf027b1  7.7300E+02  3.216E-01
*tf027b2  8.2300E+02  3.341E-01
*tf027b3  8.7300E+02  3.458E-01
*tf027b4  9.2300E+02  3.567E-01
*tf027b5  9.7300E+02  3.668E-01
*tf027b6  1.0230E+03  3.761E-01
*tf027b7  1.0730E+03  3.847E-01
*tf027b8  1.1230E+03  3.926E-01
*tf027b9  1.1730E+03  3.998E-01
*tf027c1  1.2230E+03  4.063E-01
*tf027c2  1.2730E+03  4.121E-01
*tf027c3  1.3230E+03  4.172E-01
*tf027c4  1.3730E+03  4.216E-01
*tf027c5  1.4230E+03  4.252E-01
*tf027c6  1.4730E+03  4.279E-01
*tf027c7  1.5230E+03  4.296E-01
*tf027c8  1.5600E+03  4.302E-01
*
*tf02700  thc 25    1.0      0.0   * has hg=250 for interface
*tf02701  0    0
*tf027a2  3.7300E+02  1.514E-01
*tf027a3  4.2300E+02  1.616E-01
*tf027a4  4.7300E+02  1.719E-01
*tf027a5  5.2300E+02  1.817E-01
*tf027a6  5.7300E+02  1.907E-01
*tf027a7  6.2300E+02  1.990E-01
*tf027a8  6.7300E+02  2.066E-01
*tf027a9  7.2300E+02  2.135E-01
*tf027b1  7.7300E+02  2.199E-01
*tf027b2  8.2300E+02  2.256E-01
```

```
*tf027b3  8.7300E+02  2.309E-01
*tf027b4  9.2300E+02  2.357E-01
*tf027b5  9.7300E+02  2.401E-01
*tf027b6  1.0230E+03  2.440E-01
*tf027b7  1.0730E+03  2.476E-01
*tf027b8  1.1230E+03  2.509E-01
*tf027b9  1.1730E+03  2.538E-01
*tf027c1  1.2230E+03  2.564E-01
*tf027c2  1.2730E+03  2.587E-01
*tf027c3  1.3230E+03  2.607E-01
*tf027c4  1.3730E+03  2.624E-01
*tf027c5  1.4230E+03  2.638E-01
*tf027c6  1.4730E+03  2.648E-01
*tf027c7  1.5230E+03  2.655E-01
*tf027c8  1.5600E+03  2.657E-01
*
tf02700  thc  25   1.0      0.0  * has hg=100 for interface
tf02701  0    0
tf027a2  3.7300E+02  9.156E-02
tf027a3  4.2300E+02  9.520E-02
tf027a4  4.7300E+02  9.869E-02
tf027a5  5.2300E+02  1.018E-01
tf027a6  5.7300E+02  1.046E-01
tf027a7  6.2300E+02  1.070E-01
tf027a8  6.7300E+02  1.092E-01
tf027a9  7.2300E+02  1.111E-01
tf027b1  7.7300E+02  1.128E-01
tf027b2  8.2300E+02  1.143E-01
tf027b3  8.7300E+02  1.156E-01
tf027b4  9.2300E+02  1.168E-01
tf027b5  9.7300E+02  1.179E-01
tf027b6  1.0230E+03  1.188E-01
tf027b7  1.0730E+03  1.197E-01
tf027b8  1.1230E+03  1.204E-01
tf027b9  1.1730E+03  1.211E-01
tf027c1  1.2230E+03  1.217E-01
tf027c2  1.2730E+03  1.222E-01
tf027c3  1.3230E+03  1.227E-01
tf027c4  1.3730E+03  1.230E-01
tf027c5  1.4230E+03  1.233E-01
tf027c6  1.4730E+03  1.236E-01
tf027c7  1.5230E+03  1.237E-01
tf027c8  1.5600E+03  1.238E-01
*
---
tf21812  1005.01  0.001
```